Subcomponent Validation of Composite Joints for the Marine Energy Advanced Materials Project

Paul Murdy,[1] Scott Hughes,[1] David Miller,[2] Francisco Presuel-Moreno,[3] George Bonheyo,[4] Bernadette Hernandez-Sanchez,[5] and Budi Gunawan[5]

1 National Renewable Energy Laboratory
2 Montana State University
3 Florida Atlantic University
4 Pacific Northwest National Laboratory
5 Sandia National Laboratories

NREL is a national laboratory of the U.S. Department of Energy
Office of Energy Efficiency & Renewable Energy
Operated by the Alliance for Sustainable Energy, LLC

This report is available at no cost from the National Renewable Energy Laboratory (NREL) at www.nrel.gov/publications.

Contract No. DE-AC36-08GO28308

Technical Report
NREL/TP-5700-84487
January 2023

Subcomponent Validation of Composite Joints for the Marine Energy Advanced Materials Project

Paul Murdy,[1] Scott Hughes,[1] David Miller,[2]
Francisco Presuel-Moreno,[3] George Bonheyo,[4]
Bernadette Hernandez-Sanchez,[5] and Budi Gunawan[5]

1 National Renewable Energy Laboratory
2 Montana State University
3 Florida Atlantic University
4 Pacific Northwest National Laboratory
5 Sandia National Laboratories

Suggested Citation
Murdy, Paul, Scott Hughes, David Miller, Francisco Presuel-Moreno, George Bonheyo, Bernadette Hernandez-Sanchez, and Budi Gunawan. 2023. *Subcomponent Validation of Composite Joints for the Marine Energy Advanced Materials Project*. Golden, CO: National Renewable Energy Laboratory. NREL/TP-5700-84487.
https://www.nrel.gov/docs/fy23osti/84487.pdf.

NREL is a national laboratory of the U.S. Department of Energy
Office of Energy Efficiency & Renewable Energy
Operated by the Alliance for Sustainable Energy, LLC

This report is available at no cost from the National Renewable Energy Laboratory (NREL) at www.nrel.gov/publications.

Contract No. DE-AC36-08GO28308

Technical Report
NREL/TP-5700-84487
January 2023

National Renewable Energy Laboratory
15013 Denver West Parkway
Golden, CO 80401
303-275-3000 • www.nrel.gov

NOTICE

This work was authored in part by the National Renewable Energy Laboratory, operated by Alliance for Sustainable Energy, LLC, for the U.S. Department of Energy (DOE) under Contract No. DE-AC36-08GO28308. Funding provided by U.S. Department of Energy Office of Energy Efficiency and Renewable Energy Water Power Technologies Office. The views expressed herein do not necessarily represent the views of the DOE or the U.S. Government.

Cover Photos by Dennis Schroeder: (clockwise, left to right) NREL 51934, NREL 45897, NREL 42160, NREL 45891, NREL 48097, NREL 46526.

Acknowledgments

The authors would like to thank all the affiliate laboratories, researchers, and partners that have made significant contributions to this research. We would also like to acknowledge our project leads at the U.S. Department of Energy's Water Power Technologies Office, Lauren Ruedy and Carrie Noonan, for all their guidance and valuable feedback throughout the project. Finally, this project would not have been possible without the technician support provided by Bill Gage, Mike Jenks, Sara Wallen, Victor Castillo, and David Barnes.

Sandia National Laboratories is a multi-mission laboratory managed and operated by National Technology and Engineering Solutions of Sandia, LLC., a wholly owned subsidiary of Honeywell International, Inc., for the U.S. Department of Energy's National Nuclear Security Administration under contract DE-NA0003525.

List of Acronyms

CAD	computer-aided design
CCLS	composite-composite lap shear
DEI	double-ended insert
FAU	Florida Atlantic University
ft	foot
GPa	gigapascal
Hz	hertz
in.	inch
IPA	isopropyl alcohol
lbf·ft	poundforce-foot
lbs	pounds
kip	kilopound
kN	kilonewton
m	meter
mm	millimeter
MMLS	metal-metal lap shear
MPa	megapascal
MSU	Montana State University
N·m	newton-meter
NREL	National Renewable Energy Laboratory
OBS	oversized beam shear
PNNL	Pacific Northwest National Laboratory
psi	pounds per square inch
SBS	short beam shear

Executive Summary

The Marine Energy Advanced Materials project is an ongoing, multiyear, multilaboratory project with the main goals of addressing barriers and uncertainties facing marine energy developers in adopting advanced materials for structural applications. The National Renewable Energy Laboratory's (NREL's) goals for the project were to address subcomponent testing needs for marine energy materials, improve understanding of design allowables at full scale, and provide near-net-scale static and fatigue data of composite subcomponents using materials applicable to the marine energy industry. In the long term, the test method development and data generated will be used to inform standards development. This report outlines perhaps one of the largest-scale studies conducted with regard to saltwater conditioning of various composite material subcomponents and their subsequent structural validation, specifically directed at the marine renewable energy industry.

A variety of fiberglass composite panels with epoxy and vinyl ester epoxy resin systems were manufactured at Montana State University and were then used to manufacture an array of different types of subcomponent test specimens at NREL's Flatirons Campus. These subcomponents were in the form of T-bolt and double-ended-insert specimens, which were intended to represent bonded and mechanical bolted connections for thick composite laminates, metal-metal and composite lap shear specimens to evaluate adhesion of constituent materials, and adhesive beam-shear specimens as part of an effort to better evaluate the characteristics of thick adhesive bondlines. Overall, the materials used were fiberglass reinforced epoxy and vinyl ester matrix composites, epoxy and methacrylate adhesives, and 316 and 2507 stainless steels. Specimens were then conditioned in salt water at various temperatures and for various periods of time at Florida Atlantic University and Pacific Northwest National Laboratory.

All specimens were mechanically characterized and validated using various test methods under static and fatigue loading conditions at NREL's Structural Technology Laboratory. Throughout the conditioning and mechanical validation process, valuable experience was gained, which will help guide future test method development for marine energy materials. In many instances, the results were similar to what had been observed during previous coupon-scale characterization efforts that provided a vital understanding of the scale-up process. However, in some instances, unexpected phenomena were observed, such as interactions between the adhesives and 316 steel. Furthermore, some materials exhibited significant degradation due to the saltwater conditioning.

Ultimately, this report provides a detailed summary of the specimens that were designed, the subcomponent test methods that were developed, and the results that were generated, which will serve as important guidance for marine renewable energy developers and researchers for future structural designs and validation.

Table of Contents

List of Figures

List of Tables

1 Introduction

The Marine Energy Advanced Materials project is a multiyear, multilaboratory program with the purpose of addressing barriers and uncertainties currently facing marine energy developers in using composite materials for load-bearing structures (Hernandez-Sanchez et al. 2019). The National Renewable Energy Laboratory's (NREL's) role in this program is to conduct subcomponent validation efforts with the main goals of:

- Developing subcomponent test methods for marine energy materials
- Improving understanding of design allowables for full-scale structural components and joints, which include scaling effects
- Reducing the time and cost required for full-scale structural validation
- Providing near-net-scale static and fatigue data of composite subcomponents for marine energy systems
- Building upon results from coupon-scale characterization efforts
- Including environmental effects that may not be possible for validation of complete systems
- Informing standards development early in the process by advancing the definition of a building block approach for marine energy systems.

To approach these goals, a large testing program was developed at NREL to investigate a variety of materials and design details at the subcomponent scale (Murdy and Hughes 2020) that were highlighted by industry surveys and previous coupon-scale characterization data (Miller et al. 2020). A variety of specimen geometries were designed to highlight key features of multimaterial (composite/composite or metal/composite) interconnects that may be utilized in marine energy structural designs. The designs used several different composite matrices, adhesives, and marine-grade steels, which are most appropriate for harsh marine environments. Composite panels were then manufactured by Montana State University (MSU), which were subsequently manufactured into test specimens by NREL. The specimens were shipped to Florida Atlantic University (FAU) and Pacific Northwest National Laboratory (PNNL) for conditioning in ocean water tanks at various temperatures for an extended period of time. The specimens were then returned to NREL for structural validation. The proceeding sections of this report provide detailed descriptions of the specimens, the test methods that were developed and performed, and the results and key findings from the subcomponent testing program to date.

2 Specimen Design and Manufacturing

A variety of different specimens were designed and manufactured to perform a broad spectrum of mechanical tests at the coupon and subcomponent levels before and after conditioning in saltwater tanks at various temperatures at FAU and PNNL. These included fiberglass reinforced epoxies and vinyl-esters, epoxy and methacrylate adhesives, and 316 and 2507 super-duplex stainless steels.

2.1 Panel Manufacturing at Montana State University

An array of fiberglass composite panels of varying thicknesses were manufactured at MSU under subcontract number ADJ-9-92174-01; test specimens were manufactured from these panels. Materials used in panel fabrication included resin and fiberglass. Two types of resin systems were used in panel manufacturing:

- Hexion 035 (epoxy)
    - Epikote Resin MGS RIMR 035c
    - Lot LL5AG18F
    - 32 gallons of resin
    - 13 gallons of 035c Part B
    - Hexion mix ratio was 100:28 by weight
- Derakane 411C-350 (Vinylester-epoxy)
    - 8 gallons.

Vectorply was the supplier for the fiberglass fabric used to construct the panels. Vectorply E-QX 9000 fabric was used in all panels. The E-QX 9000 fabric is quadriaxial (0, 45, 90, −45). Rolls of fabric were 24 yards long by 50 inches (in.) wide. 11 rolls were used to manufacture the panels. The ply thickness of the E-QX 9000 fabric was about 1.92 millimeters (mm).

Resin infusion techniques were used to manufacture the panels. Figure 1 shows the manufacturing setup used at MSU. A large aluminum plate was polished and served as the A-side of the mold. Heating pads were mounted underneath the aluminum plate for post-curing. Thermocouples measured the post-cure temperature on the top and bottom surface of the panel. 5-foot (ft) by 8-ft by 1/2-in. aluminum was used for caul plates. Additional materials used for manufacturing included bagging, tacky tape, flow media, peel ply, and general shop supplies. The volume fraction was somewhat higher than expected, near 58% fiber volume. Figure 2 shows a cross-sectional view of one of the thicker panels manufactured, and Figure 3 shows two complete panels. Table 1 provides a summary of the manufactured composite panels, as well as their matrix materials, dimensions, and weights.

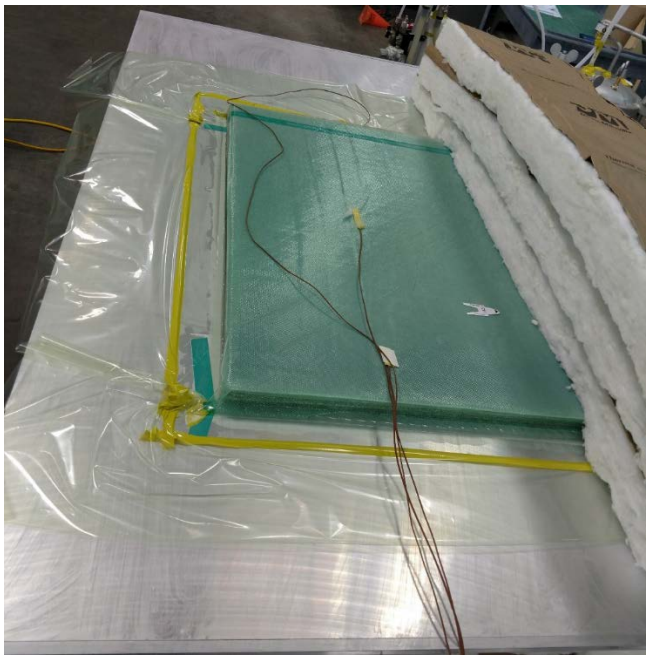

Figure 1. The panel manufacturing setup used at MSU

Figure 2. Cross-sectional view of a manufactured thick panel

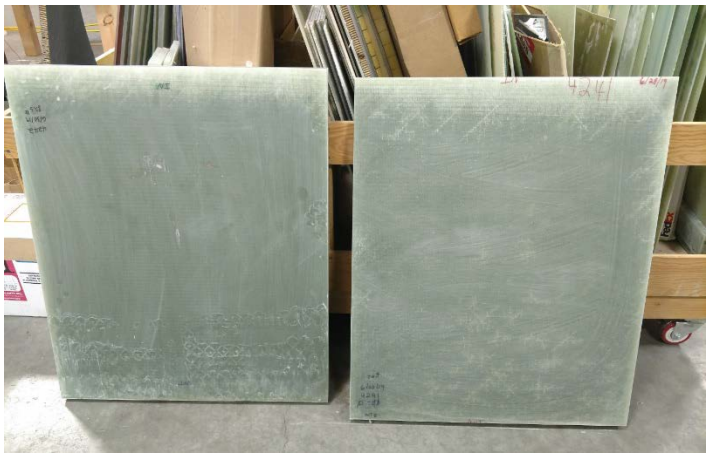

Figure 3. Two complete panels

Table 1. A Summary of the Composite Panels Manufactured at MSU

Panel Number	Matrix Material	Width (mm)	Length (mm)	Thickness (mm)	Weight (kg)
4241	Hexion	609	730	43	39
4242	Hexion	619	736	43	39
4243	Hexion	612	895	43	47
4245	Derakane	600	886	43	45
4247	Hexion	610	875	82	88
4248	Hexion	612	730	82	75
4250	Derakane	620	741	82	75
4251	Hexion	620	745	84	77
4252	Derakane	621	745	86	78
4254	Hexion	630	1,160	12	25
4255	Hexion	630	1,160	12	25
4257	Hexion	630	1,160	12	25
4258	Hexion	630	1,160	12	25
4259	Hexion	630	1,160	4	9
4260	Hexion	630	1,160	4	9
4261	Hexion	630	1,160	12	25
4262	Derakane	630	1,160	4	9
4263	Derakane	630	1,160	12	25
4264	Derakane	630	1,160	12	25
4265	Derakane	630	1,160	4	9

2.2 T-Bolt Specimens

The T-bolt specimens were designed to be characterized in the 500-kilonewton (kN) load frame in NREL's Structural Technology Laboratory. The specimens were intended to represent mechanical interconnects used to join thick composites with dissimilar materials, such as metal structures. These types of connections are one common method that have been used at the root end of wind turbine blades to join them to the hub (Lee, Kang, and Park 2015; Bahri, Salehi, and Akhlaghi 2014; Ashworth Briggs, Y. Zhang, and Dhakal 2014). T-bolt joints may also be used to mechanically join composite-to-composite structures. T-bolt joints may be a useful alternative to adhesive joints for marine energy system designers and developers.

Figure 4 shows a computer-aided design (CAD) drawing of the final T-bolt specimen dimensions as designed. Specimens were manufactured by first cutting 80 × 300-mm blanks from the 43-mm-thick Hexion and Derakane panels (panel numbers 4241 to 4245) by waterjet cutting. They were then sent to a machine shop for milling the holes and facing the end surfaces to be flat within 0.5 mm, parallel within 0.1 mm of each other, and perpendicular to the mold side surface within 0.1 mm. A total of 28 specimens were manufactured: 14 Hexion epoxy and 14 Derakane vinyl ester. The dimensions shown in Figure 4 were unchanged for specimen static testing; however, the widths of the specimens for fatigue testing were reduced from 80 mm to 52 mm.

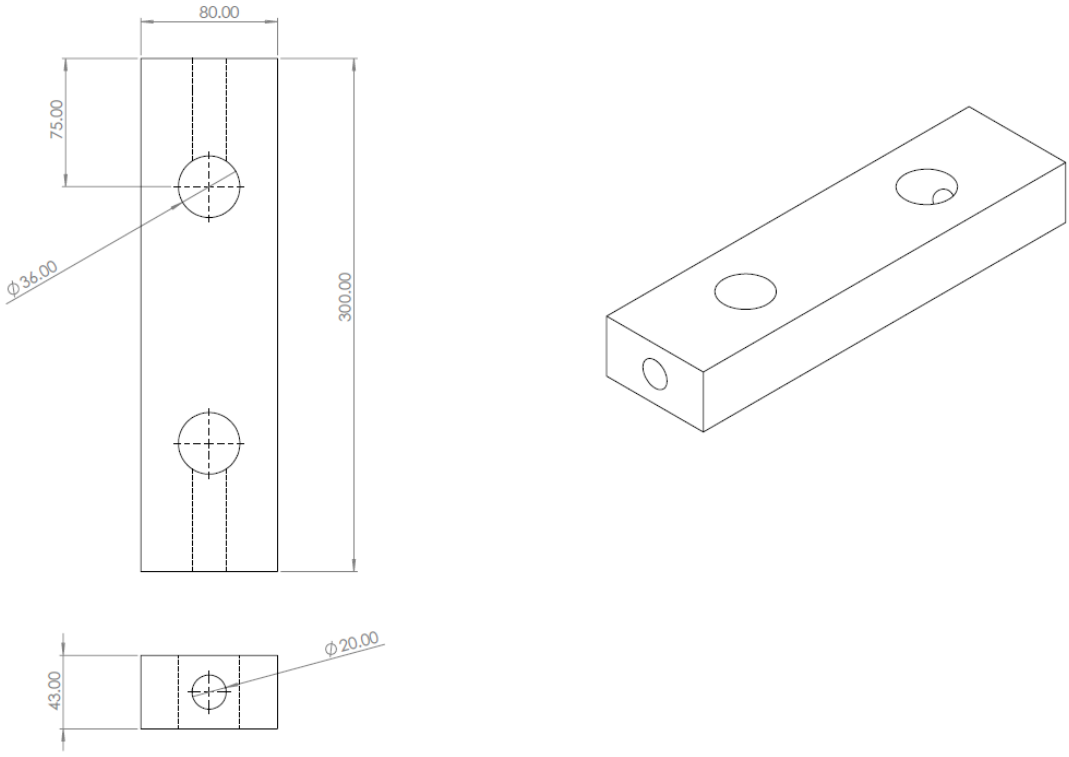

Figure 4. CAD drawing of T-bolt specimens (dimensions in millimeters)

For the specimens that were to be conditioned in the tanks at PNNL and FAU, hardware was designed to apply realistic preloads to the specimens while also allowing water to easily enter the cavities (Figure 5). The preload plates were machined from 4140 carbon steel, and the barrel nuts and M20 socket head cap screws were made of 316 stainless steel. Fiber optic strain sensors

were bonded to some of the specimens so that strain measurements could be taken throughout the duration of the environmental conditioning testing conduced at PNNL and FAU. Sensors were bonded using Marine-Tex epoxy putty at locations equidistant between the through-hole and compression plate and equidistant between the through-hole and the side of specimens (Figure 5). The socket head cap screws were torqued to 100 pound-force feet (lbf·ft) (136 newton-meters [N·m]) with Teflon tape while recording strain data and shipped to the respective laboratories for in-water conditioning (Figure 6). Table 2 provides a summary of the manufactured specimens, the matrix materials used, their conditioning locations, and the test method applied to them (static or fatigue).

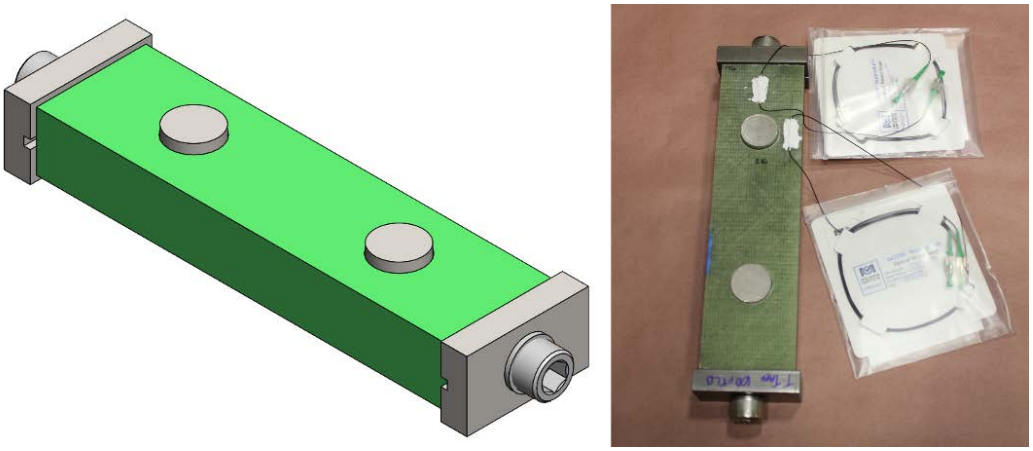

Figure 5. (left) CAD drawing of a specimen assembled for in-water conditioning and (right) a photo of an assembled specimen with fiber optic strain gauges bonded

Figure 6. T-bolt specimens packaged and ready to be shipped to PNNL and FAU

Table 2. A Comprehensive List of the T-Bolt Specimens Manufactured and the Materials Used

Specimen Name	Matrix Material	Conditioning Location	Loading Applied
TB-H01	Hexion	FAU	Static
TB-H02	Hexion	FAU	Static
TB-H03	Hexion	FAU	Fatigue
TB-H04	Hexion	FAU	Fatigue
TB -H05	Hexion	FAU	Fatigue
TB -H06	Hexion	PNNL	Static
TB -H07	Hexion	PNNL	Static
TB -H08	Hexion	PNNL	Fatigue
TB -H09	Hexion	PNNL	Fatigue
TB -H10	Hexion	PNNL	Fatigue
TB -H11	Hexion	-	Fatigue
TB -H12	Hexion	-	Fatigue
TB -H13	Hexion	-	Static
TB -H14	Hexion	-	Static
TB -D01	Derakane	FAU	Static
TB -D02	Derakane	-	-
TB -D03	Derakane	FAU	Static
TB -D04	Derakane	FAU	Fatigue
TB -D05	Derakane	FAU	Fatigue
TB -D06	Derakane	PNNL	Static
TB -D07	Derakane	PNNL	Static
TB-D08	Derakane	PNNL	Fatigue
TB-D09	Derakane	PNNL	Fatigue
TB-D10	Derakane	PNNL	Fatigue
TB-D11	Derakane	-	Fatigue
TB-D12	Derakane	-	Fatigue
TB-D13	Derakane	-	Static
TB-D14	Derakane	-	Static

2.3 Double-Ended-Insert Specimens

The double-ended-insert (DEI) specimens were also designed to be characterized in the 500-kN load frame at NREL's Structural Technology Laboratory. These specimens were also designed to be an alternative mechanical interconnect architecture for joining thick composite laminates with dissimilar material structures. The DEI specimens consisted of threaded cylindrical steel inserts

that were adhesively bonded in-plane with the composite laminate direction. This is also a commonly used design for the root end of wind turbine blades to attach them to the hub (Bender, Hallett, and Lindgaard 2019; Murdy et al. 2021). The specimen dimensions were based around the design of the root connections of the National Rotor Testbed 13-meter (m) blades (Figure 7) (Ennis and Paquette 2015). The steel inserts were machined from 316 stainless steel and 2507 super-duplex steel and were designed to be used for M20 studs.

For load frame characterization, it was critical to maintain good dimensional tolerances to appropriately align the specimens within the load frame. Good tolerances were defined as insert end faces being parallel within 0.03 mm and concentric within 0.05 mm. To meet these specifications, several machining and bonding steps and bespoke fixturing were required to manufacture the specimens.

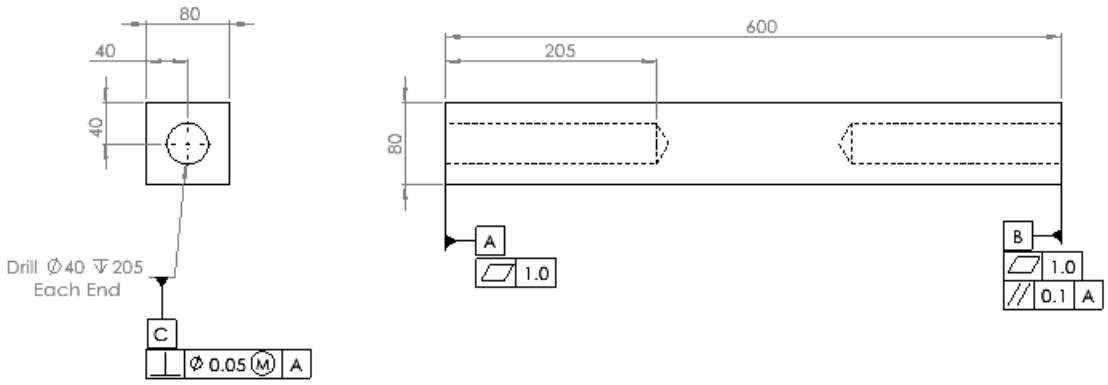

Figure 7. Cross-sectional and end-view drawings of the composite portion of the DEI specimens as designed (dimensions in millimeters)

First, the 80-mm-thick panels (panel numbers 4247 to 4252) were waterjet cut to 600 × 610-mm blanks. These blanks were then sent to a machine shop to have 7 holes bored on either end to accommodate the adhesively bonded steel inserts so that each blank would yield seven DEI specimens (Figure 8). Two 12-mm holes were drilled on each end to be used for alignment pins with a specifically designed bonding fixture. Also, pin holes were drilled through the surface at each insert hole to allow squeeze-out of excess adhesive during the bonding process. Finally, the ends of the blanks were faced flat to be parallel within 0.5 mm.

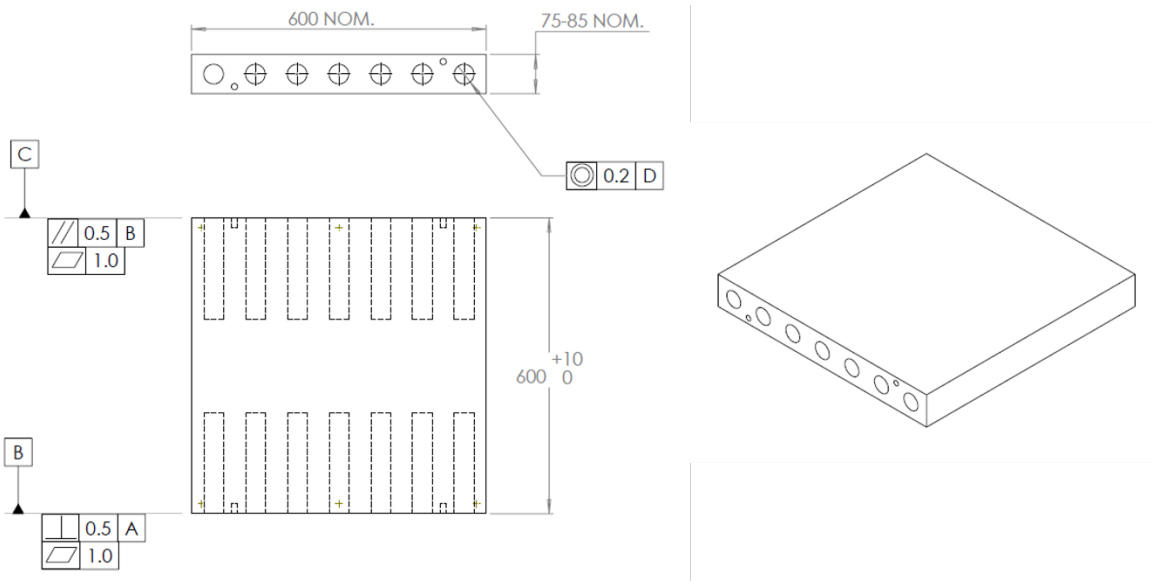

Figure 8. CAD drawing of the large composite blanks after machining (dimensions in millimeters)

Figure 9 shows the adhesive bonding fixture as designed. It was intended that seven inserts could be bonded into each end of a composite blank at the same time. The baseplate was 12.5-mm-thick aluminum and had channels machined in it to fixture rails to a flat surface. The end plates were also machined from 75 × 100 aluminum bar stock. The in-facing surfaces were machined to be perpendicular with the bottom surface within 0.1 mm. The inserts were to be bolted to these faces with injection bolts (Figure 10)—hollow M20 bolts specifically designed for injecting adhesives to fill the cavity between the inserts and the composite. The two end bars were aligned with the composite blank using 12-mm alignment pins and 1.5-in. Acme screws on either side of the blank. They were used to clamp the end bars to the composite blanks; good alignment was ensured by measuring the distances between each side of the end bars. Silicone gaskets were used between the end bars and the composite blank to control squeeze-out of the adhesive and prevent the end bars from bonding to the composite.

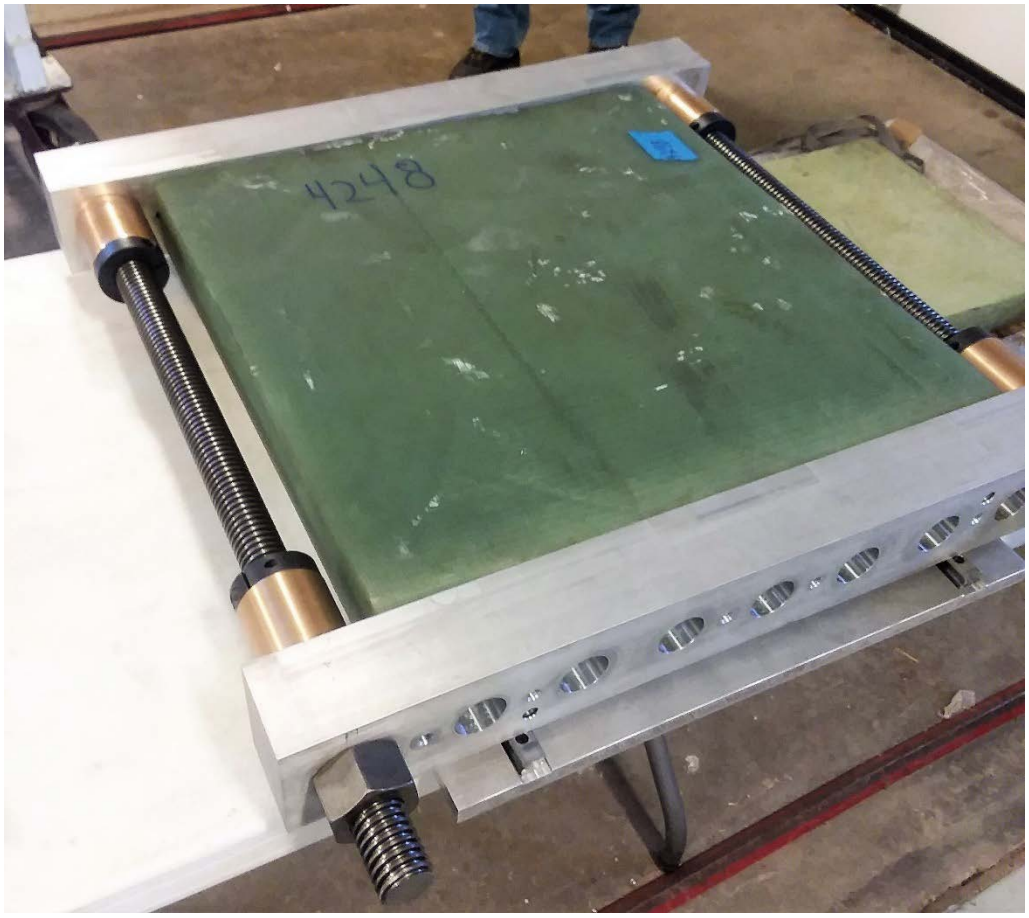

Figure 9. The fixture used to adhesively bond the steel inserts into the thick composite blanks

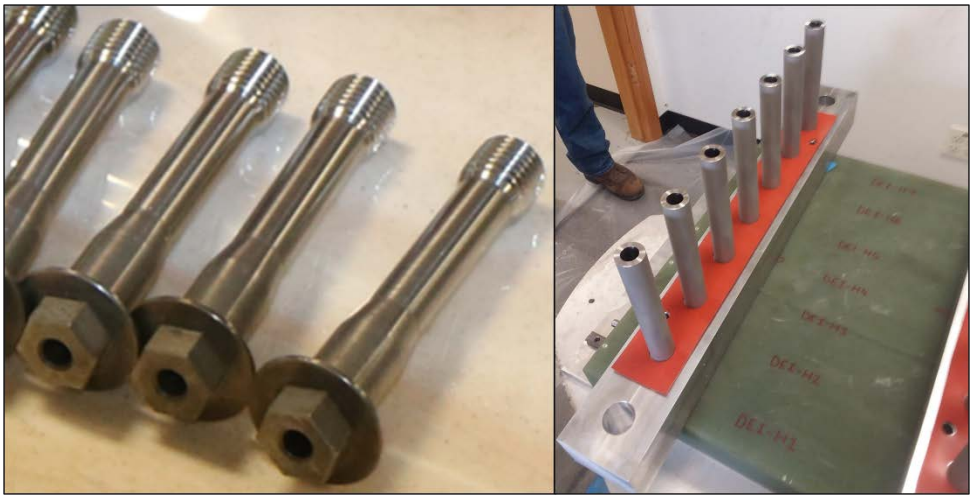

Figure 10. (left) An M20 injection bolt used to inject adhesive into the cavity between the inserts and the composite blank and (right) a photo of the inserts bolted to the end bars in preparation for bonding

Two different adhesives were used for this study:

1. Araldite 2015, an epoxy adhesive
2. Plexus MA560-1, a methyl-methacrylate adhesive.

Before bonding, the steel inserts were prepared by sandblasting and cleaning with isopropyl-alcohol (IPA). The inserts to be bonded with the Plexus adhesive were then wiped with a thin coat of Plexus PC120 primer. The holes in the composite blanks were also prepared by wiping them with IPA.

Once the steel inserts were assembled and ready for bonding, adhesive was injected through the injection bolts using a pneumatic dispensing gun with mixing nozzles to properly mix the two-part adhesives. Adhesive was injected until it squeezed out of the exit holes drilled on the surface of the composite panel, so the cavity between the steel inserts and the composite was filled with adhesive without any air bubbles or voids. The adhesive cartridges were weighed before and after each hole was filled for quality assurance purposes. The adhesive was left to cure before disassembly of the fixture (Figure 11).

Figure 11. A composite blank with the adhesive bonding process complete

Finally, the large composite panels were waterjet cut to yield seven DEI specimens each (Figure 12). Prior to shipping to PNNL and FAU, M20 bolts with rubber gaskets were installed in both ends of the specimen to protect the insert threads from corrosion during saltwater conditioning. Table 3 provides a summary of the composite matrices, steel insert materials, and adhesives used for each DEI specimen for this study.

Figure 12. Complete DEI specimens ready to be shipped to FAU and PNNL

Table 3. A Comprehensive List of the DEI Specimens Manufactured and the Materials Used

Specimen Name	Matrix Material	Insert Steel	Adhesive	Conditioning Location
DEI-H01	Hexion	316	Araldite 2015	-
DEI-H02	Hexion	316	Araldite 2015	FAU
DEI-H03	Hexion	316	Araldite 2015	FAU
DEI-H04	Hexion	316	Araldite 2015	PNNL
DEI-H05	Hexion	316	Araldite 2015	PNNL
DEI-H06	Hexion	2507	Araldite 2015	FAU
DEI-H07	Hexion	2507	Araldite 2015	PNNL
DEI-H08	Hexion	2507	Plexus MA560-1	-
DEI-H09	Hexion	2507	Plexus MA560-1	FAU
DEI-H10	Hexion	2507	Plexus MA560-1	FAU
DEI-H11	Hexion	2507	Plexus MA560-1	FAU
DEI-H12	Hexion	2507	Plexus MA560-1	PNNL
DEI-H13	Hexion	316	Plexus MA560-1	PNNL
DEI-H14	Hexion	316	Plexus MA560-1	-
DEI-D01	Derakane	316	Araldite 2015	FAU
DEI-D02	Derakane	316	Araldite 2015	PNNL
DEI-D03	Derakane	2507	Araldite 2015	-
DEI-D04	Derakane	2507	Araldite 2015	FAU
DEI-D05	Derakane	2507	Araldite 2015	PNNL
DEI-D06	Derakane	316	Plexus MA560-1	FAU
DEI-D07	Derakane	other	Araldite 2015	PNNL

2.4 Lap Shear Specimens

Lap shear specimens were manufactured to compare and quantify the quality of adhesion of the Araldite and Plexus adhesives with the composite and metallic materials used to manufacture the DEI specimens. Therefore, composite-composite lap shear (CCLS) specimens and metal-metal lap shear (MMLS) specimens were manufactured. The specimen geometries were generally based on recommendations from ASTM D1003-10 and ASTM D3163-01 standard test methods. Figure 13 shows the dimensions of the manufactured lap shear specimens. All specimens were intended to have a 3-mm-thick and 25-mm-long bondline for comparison to the DEI specimens.

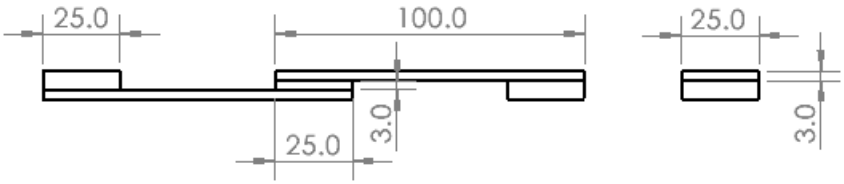

Figure 13. CAD drawing showing the dimensions of the lap shear specimens as manufactured (all dimensions in millimeters)

To produce the MMLS specimens, 1/8-in.-thick steel panels were cut into 150 × 300-mm blanks. Along the long edges of the blanks, 25-mm strips were taped off and sandblasted, then wiped with IPA to prepare the surfaces for bonding. For the CCLS specimens, panels 4260 and 4265 were cut into 150 × 300-mm blanks. Like the MMLS blanks, 25-mm bonding surfaces were taped off and wiped with IPA to prepare them for bonding. The MMLS blanks being bonded with the Plexus adhesive were also wiped with a thin layer of the Plexus PC120 primer. Blue flash tape was used to control the width of the bondline and prevent the adhesive from sticking to unwanted areas. Panels were bonded together with a single bead of adhesive to prevent voids in the bondline and the thickness was controlled using nylon shims at either end of each panel. The blanks were then clamped together and left to cure. Figure 14 shows MMLS blanks bonded together and cured. After bonding, the metal blanks were waterjet cut to yield the MMLS specimens, and the composite blanks were cut on a water-cooled diamond tile saw to yield the final CCLS specimens (Figure 15). Table 4 and Table 5 provide a comprehensive overview of all the MMLS and CCLS specimens manufactured.

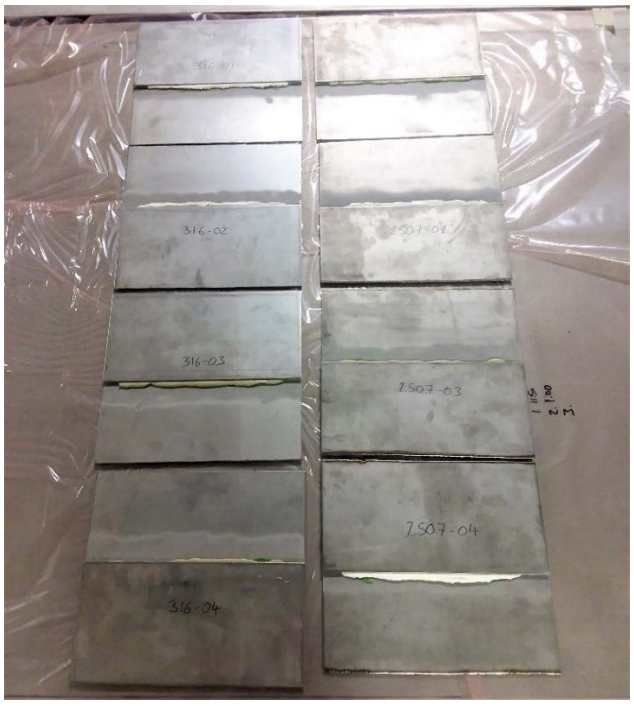

Figure 14. MMLS blanks bonded together before being waterjet cut to produce the MMLS specimens

Figure 15. (top) The final manufactured MMLS and CCLS specimens and (bottom) a closer view of a CCLS bondline cross section

Table 4. A Comprehensive List of the MMLS Specimens Manufactured and the Materials Used

Specimen Name	Steel	Adhesive	Conditioning Location
316-01-01	316	Plexus MA560-1	FAU
316-01-02	316	Plexus MA560-1	FAU
316-01-03	316	Plexus MA560-1	FAU
316-01-04	316	Plexus MA560-1	FAU
316-01-05	316	Plexus MA560-1	-
316-01-06	316	Plexus MA560-1	-
316-01-07	316	Plexus MA560-1	-
316-01-08	316	Plexus MA560-1	-
316-01-09	316	Plexus MA560-1	-
316-01-10	316	Plexus MA560-1	-
316-02-01	316	Plexus MA560-1	PNNL
316-02-02	316	Plexus MA560-1	PNNL
316-02-03	316	Plexus MA560-1	PNNL
316-02-04	316	Plexus MA560-1	PNNL
316-02-05	316	Plexus MA560-1	-

Specimen Name	Steel	Adhesive	Conditioning Location
316-02-06	316	Plexus MA560-1	-
316-02-07	316	Plexus MA560-1	-
316-02-08	316	Plexus MA560-1	-
316-02-09	316	Plexus MA560-1	-
316-02-10	316	Plexus MA560-1	-
316-03-01	316	Araldite 2015	FAU
316-03-02	316	Araldite 2015	FAU
316-03-03	316	Araldite 2015	FAU
316-03-04	316	Araldite 2015	-
316-03-05	316	Araldite 2015	FAU
316-03-06	316	Araldite 2015	-
316-03-07	316	Araldite 2015	-
316-03-08	316	Araldite 2015	-
316-03-09	316	Araldite 2015	-
316-03-10	316	Araldite 2015	-
316-04-01	316	Araldite 2015	-
316-04-02	316	Araldite 2015	PNNL
316-04-03	316	Araldite 2015	PNNL
316-04-04	316	Araldite 2015	PNNL
316-04-05	316	Araldite 2015	PNNL
316-04-06	316	Araldite 2015	-
316-04-07	316	Araldite 2015	-
316-04-08	316	Araldite 2015	-
316-04-09	316	Araldite 2015	-
316-04-10	316	Araldite 2015	-
2507-01-01	2507	Araldite 2015	FAU
2507-01-02	2507	Araldite 2015	FAU
2507-01-03	2507	Araldite 2015	FAU
2507-01-04	2507	Araldite 2015	FAU
2507-01-05	2507	Araldite 2015	-
2507-01-06	2507	Araldite 2015	-
2507-01-07	2507	Araldite 2015	-
2507-01-08	2507	Araldite 2015	-
2507-01-09	2507	Araldite 2015	-
2507-01-10	2507	Araldite 2015	-

Specimen Name	Steel	Adhesive	Conditioning Location
2507-02-01	2507	Plexus MA560-1	FAU
2507-02-02	2507	Plexus MA560-1	FAU
2507-02-03	2507	Plexus MA560-1	FAU
2507-02-04	2507	Plexus MA560-1	FAU
2507-02-05	2507	Plexus MA560-1	-
2507-02-06	2507	Plexus MA560-1	-
2507-02-07	2507	Plexus MA560-1	-
2507-02-08	2507	Plexus MA560-1	-
2507-02-09	2507	Plexus MA560-1	-
2507-02-10	2507	Plexus MA560-1	-
2507-03-01	2507	Araldite 2015	-
2507-03-02	2507	Araldite 2015	-
2507-03-03	2507	Araldite 2015	-
2507-03-04	2507	Araldite 2015	-
2507-03-05	2507	Araldite 2015	-
2507-03-06	2507	Araldite 2015	PNNL
2507-03-07	2507	Araldite 2015	PNNL
2507-03-08	2507	Araldite 2015	PNNL
2507-03-09	2507	Araldite 2015	PNNL
2507-03-10	2507	Araldite 2015	-
2507-04-01	2507	Plexus MA560-1	PNNL
2507-04-02	2507	Plexus MA560-1	PNNL
2507-04-03	2507	Plexus MA560-1	PNNL
2507-04-04	2507	Plexus MA560-1	PNNL
2507-04-05	2507	Plexus MA560-1	-
2507-04-06	2507	Plexus MA560-1	-
2507-04-07	2507	Plexus MA560-1	-
2507-04-08	2507	Plexus MA560-1	-
2507-04-09	2507	Plexus MA560-1	-
2507-04-10	2507	Plexus MA560-1	-

Table 5. A Comprehensive List of the CCLS Specimens Manufactured and the Materials Used

Specimen Name	Matrix Material	Adhesive	Conditioning Location
CCLS-01	Hexion	Araldite 2015	FAU
CCLS-02	Hexion	Araldite 2015	FAU
CCLS-03	Hexion	Araldite 2015	FAU
CCLS-04	Hexion	Araldite 2015	PNNL
CCLS-05	Hexion	Araldite 2015	PNNL
CCLS-06	Hexion	Araldite 2015	PNNL
CCLS-07	Hexion	Araldite 2015	-
CCLS-08	Hexion	Araldite 2015	-
CCLS-09	Hexion	Araldite 2015	-
CCLS-10	Hexion	Araldite 2015	-
CCLS-11	Derakane	Araldite 2015	FAU
CCLS-12	Derakane	Araldite 2015	FAU
CCLS-13	Derakane	Araldite 2015	FAU
CCLS-14	Derakane	Araldite 2015	PNNL
CCLS-15	Derakane	Araldite 2015	PNNL
CCLS-16	Derakane	Araldite 2015	-
CCLS-17	Derakane	Araldite 2015	PNNL
CCLS-18	Derakane	Araldite 2015	-
CCLS-19	Derakane	Araldite 2015	-
CCLS-20	Derakane	Araldite 2015	-
CCLS-21	Hexion	Plexus MA560-1	FAU
CCLS-22	Hexion	Plexus MA560-1	FAU
CCLS-23	Hexion	Plexus MA560-1	-
CCLS-24	Hexion	Plexus MA560-1	FAU
CCLS-25	Hexion	Plexus MA560-1	PNNL
CCLS-26	Hexion	Plexus MA560-1	PNNL
CCLS-27	Hexion	Plexus MA560-1	PNNL
CCLS-28	Hexion	Plexus MA560-1	-
CCLS-29	Hexion	Plexus MA560-1	-
CCLS-30	Hexion	Plexus MA560-1	-
CCLS-31	Derakane	Plexus MA560-1	FAU
CCLS-32	Derakane	Plexus MA560-1	FAU
CCLS-33	Derakane	Plexus MA560-1	FAU
CCLS-34	Derakane	Plexus MA560-1	PNNL

Specimen Name	Matrix Material	Adhesive	Conditioning Location
CCLS-35	Derakane	Plexus MA560-1	PNNL
CCLS-36	Derakane	Plexus MA560-1	-
CCLS-37	Derakane	Plexus MA560-1	PNNL
CCLS-38	Derakane	Plexus MA560-1	-
CCLS-39	Derakane	Plexus MA560-1	-
CCLS-40	Derakane	Plexus MA560-1	-

2.5 Beam Shear Specimens

As an alternative to characterizing thick adhesive shear strengths using lap shear tests, beam shear specimens were also designed and manufactured. The specimens were generally based on the ASTM D2344-16 Standard Test Method for Short-Beam Strength of Polymer Matrix Composite Materials and their Laminates. Specimens for short-span three-point bending tests were manufactured at two different scales and with multiple layers of composite and adhesive to observe scaling effects and the effects of combined shear and axial stresses. The two scales of specimens were denoted as short-beam-shear (SBS) and oversized-beam-shear (OBS) specimens. The SBS specimens used the thinnest panels supplied by MSU (panels 4259 and 4262), and the OBS specimens used the 12-mm-thick panels supplied by MSU (panels 4254, 4255, 4263, and 4264).

Some specimens were manufactured with two layers of composite with a layer of thick adhesive between them, and others were manufactured with three layers of composite laminate and two layers of thick adhesive bonding them together. For the SBS specimens, the panels were first cut into 300 × 150-mm blanks. For the OBS specimens, the panels were cut into 650 × 75-mm blanks. All panel surfaces were prepared for adhesive bonding using the same procedures outlined for the DEI and CCLS specimens. The composite blanks were bonded together as shown in Figure 16. Again, 3-mm-thick nylon spacers were used to hold constant 3-mm-thick bondlines. The blanks were clamped together using nuts and bolts while the adhesive cured.

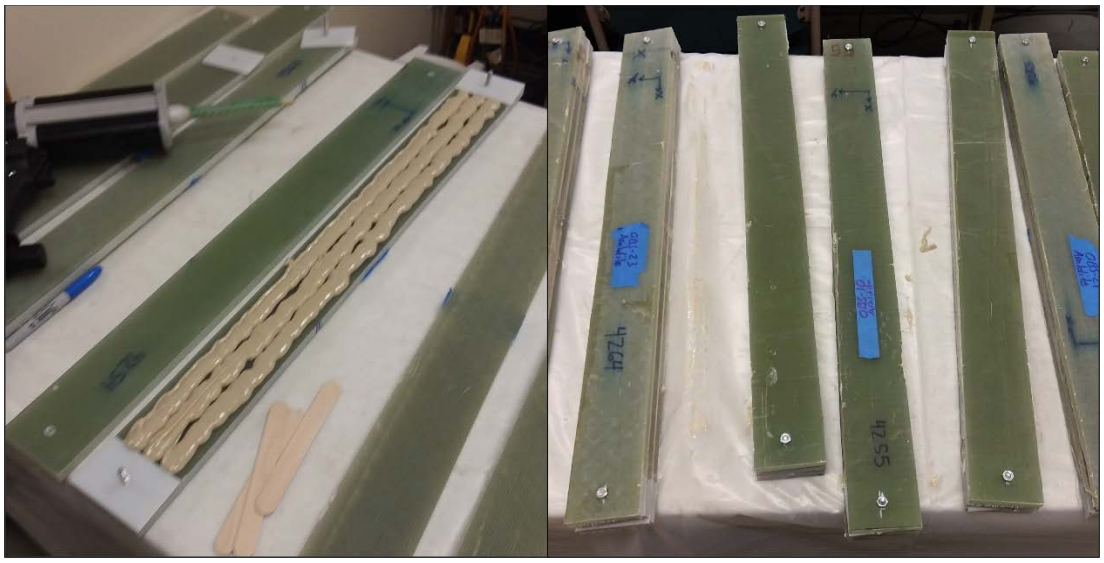

Figure 16. OBS composite blanks being (left) adhesively bonded and (right) bolted together while curing

Finally, the bonded panels were cut to their final dimensions using a water-cooled diamond tile saw. The final dimensions of the SBS specimens were 100 mm long by 25 mm wide, and the final dimensions of the OBS specimens were 600 mm long by 40 mm wide. Prior to mechanical characterization, the OBS specimens were cut to 300-mm lengths to yield double the number of test specimens. Figure 17 shows some of the final manufactured SBS and OBS specimens and Table 6 and Table 7 provide a comprehensive overview of the SBS and OBS specimens that were manufactured.

Figure 17. Some of the manufactured specimens: (left) SBS specimens; (right) OBS specimens

Table 6. A Comprehensive List of the SBS Specimens Manufactured and the Materials Used

Specimen Name	Matrix Material	Adhesive	Composite Layers	Conditioning Location
SBS-01	Hexion	Araldite 2015	2	FAU
SBS-02	Hexion	Araldite 2015	2	FAU
SBS-03	Hexion	Araldite 2015	2	FAU
SBS-04	Hexion	Araldite 2015	2	PNNL
SBS-05	Hexion	Araldite 2015	2	PNNL
SBS-06	Hexion	Araldite 2015	2	PNNL
SBS-07	Hexion	Araldite 2015	2	-
SBS-08	Hexion	Araldite 2015	2	-
SBS-09	Hexion	Araldite 2015	2	-
SBS-10	Hexion	Araldite 2015	2	-
SBS-11	Derakane	Araldite 2015	2	FAU
SBS-12	Derakane	Araldite 2015	2	FAU
SBS-13	Derakane	Araldite 2015	2	FAU
SBS-14	Derakane	Araldite 2015	2	PNNL
SBS-15	Derakane	Araldite 2015	2	PNNL
SBS-16	Derakane	Araldite 2015	2	PNNL
SBS-17	Derakane	Araldite 2015	2	-
SBS-18	Derakane	Araldite 2015	2	-
SBS-19	Derakane	Araldite 2015	2	-
SBS-20	Derakane	Araldite 2015	2	-
SBS-21	Hexion	Araldite 2015	3	FAU
SBS-22	Hexion	Araldite 2015	3	FAU
SBS-23	Hexion	Araldite 2015	3	FAU
SBS-24	Hexion	Araldite 2015	3	PNNL
SBS-25	Hexion	Araldite 2015	3	PNNL
SBS-26	Hexion	Araldite 2015	3	PNNL
SBS-27	Hexion	Araldite 2015	3	-
SBS-28	Hexion	Araldite 2015	3	-
SBS-29	Hexion	Araldite 2015	3	-
SBS-30	Hexion	Araldite 2015	3	-
SBS-31	Derakane	Araldite 2015	3	FAU
SBS-32	Derakane	Araldite 2015	3	FAU
SBS-33	Derakane	Araldite 2015	3	FAU
SBS-34	Derakane	Araldite 2015	3	PNNL

Specimen Name	Matrix Material	Adhesive	Composite Layers	Conditioning Location
SBS-35	Derakane	Araldite 2015	3	PNNL
SBS-36	Derakane	Araldite 2015	3	PNNL
SBS-37	Derakane	Araldite 2015	3	-
SBS-38	Derakane	Araldite 2015	3	-
SBS-39	Derakane	Araldite 2015	3	-
SBS-40	Derakane	Araldite 2015	3	-
SBS-41	Hexion	Plexus MA560-1	2	FAU
SBS-42	Hexion	Plexus MA560-1	2	FAU
SBS-43	Hexion	Plexus MA560-1	2	FAU
SBS-44	Hexion	Plexus MA560-1	2	PNNL
SBS-45	Hexion	Plexus MA560-1	2	PNNL
SBS-46	Hexion	Plexus MA560-1	2	PNNL
SBS-47	Hexion	Plexus MA560-1	2	-
SBS-48	Hexion	Plexus MA560-1	2	-
SBS-49	Hexion	Plexus MA560-1	2	-
SBS-50	Hexion	Plexus MA560-1	2	-
SBS-51	Derakane	Plexus MA560-1	2	FAU
SBS-52	Derakane	Plexus MA560-1	2	FAU
SBS-53	Derakane	Plexus MA560-1	2	FAU
SBS-54	Derakane	Plexus MA560-1	2	PNNL
SBS-55	Derakane	Plexus MA560-1	2	PNNL
SBS-56	Derakane	Plexus MA560-1	2	PNNL
SBS-57	Derakane	Plexus MA560-1	2	-
SBS-58	Derakane	Plexus MA560-1	2	-
SBS-59	Derakane	Plexus MA560-1	2	-
SBS-60	Derakane	Plexus MA560-1	2	-
SBS-61	Hexion	Plexus MA560-1	3	FAU
SBS-62	Hexion	Plexus MA560-1	3	FAU
SBS-63	Hexion	Plexus MA560-1	3	FAU
SBS-64	Hexion	Plexus MA560-1	3	PNNL
SBS-65	Hexion	Plexus MA560-1	3	PNNL
SBS-66	Hexion	Plexus MA560-1	3	PNNL
SBS-67	Hexion	Plexus MA560-1	3	-
SBS-68	Hexion	Plexus MA560-1	3	-
SBS-69	Hexion	Plexus MA560-1	3	-

Specimen Name	Matrix Material	Adhesive	Composite Layers	Conditioning Location
SBS-70	Hexion	Plexus MA560-1	3	-
SBS-71	Derakane	Plexus MA560-1	3	FAU
SBS-72	Derakane	Plexus MA560-1	3	FAU
SBS-73	Derakane	Plexus MA560-1	3	FAU
SBS-74	Derakane	Plexus MA560-1	3	PNNL
SBS-75	Derakane	Plexus MA560-1	3	PNNL
SBS-76	Derakane	Plexus MA560-1	3	PNNL
SBS-77	Derakane	Plexus MA560-1	3	-
SBS-78	Derakane	Plexus MA560-1	3	-
SBS-79	Derakane	Plexus MA560-1	3	-
SBS-80	Derakane	Plexus MA560-1	3	-

Table 7. A Comprehensive List of the OBS Specimens Manufactured and the Materials Used

Specimen Name	Matrix Material	Adhesive	Composite Layers	Conditioning Location
OBS-01	Hexion	Araldite 2015	2	FAU
OBS-02	Hexion	Araldite 2015	2	PNNL
OBS-03	Hexion	Araldite 2015	2	-
OBS-04	Hexion	Araldite 2015	2	-
OBS-05	Hexion	Plexus MA560-1	2	FAU
OBS-06	Hexion	Plexus MA560-1	2	PNNL
OBS-07	Hexion	Plexus MA560-1	2	-
OBS-08	Hexion	Araldite 2015	3	FAU
OBS-09	Hexion	Araldite 2015	3	PNNL
OBS-10	Hexion	Araldite 2015	3	-
OBS-11	Hexion	Plexus MA560-1	3	FAU
OBS-12	Hexion	Plexus MA560-1	3	PNNL
OBS-13	Hexion	Plexus MA560-1	3	-
OBS-14	Derakane	Araldite 2015	2	FAU
OBS-15	Derakane	Araldite 2015	2	PNNL
OBS-16	Derakane	Araldite 2015	2	-
OBS-17	Derakane	Plexus MA560-1	2	FAU
OBS-18	Derakane	Plexus MA560-1	2	PNNL
OBS-19	Derakane	Plexus MA560-1	2	-
OBS-20	Derakane	Plexus MA560-1	2	-
OBS-21	Derakane	Araldite 2015	3	FAU
OBS-22	Derakane	Araldite 2015	3	PNNL
OBS-23	Derakane	Araldite 2015	3	-
OBS-24	Derakane	Plexus MA560-1	3	FAU
OBS-25	Derakane	Plexus MA560-1	3	PNNL
OBS-26	Derakane	Plexus MA560-1	3	-

3 Experimental Characterization and Validation

The specimens described in the previous section were subjected to a variety of experimental procedures to characterize their responses to saltwater conditioning and the effects of the conditioning on mechanical strengths.

3.1 Water Absorption

A large proportion of the specimens that were manufactured were subjected to saltwater conditioning for extended periods of time. Some specimens were sent to laboratories at FAU for conditioning in Atlantic Ocean water, some were sent to PNNL's Sequim Campus for conditioning in Pacific Ocean water, and some remained at NREL's Flatirons Campus to be used as dry control specimens.

All specimen masses and their accompanying hardware were recorded and documented prior to them being shipped for testing. The specimens conditioned at FAU were soaked in tanks at an elevated temperature of 58°C to accelerate the aging process. Periodic mass measurements were taken for some of the T-bolt specimens to track the water absorption process (Nunemaker et al. 2018).

The specimens conditioned at PNNL were soaked in tanks at ambient temperatures, which allowed for natural microbial life to be present. As mentioned in Section 2.2, some of the T-bolt specimens were instrumented with fiber optic strain sensors. Periodic strain measurements were taken with a fiber optic interrogator throughout the conditioning period of those specimens.

Specimens were shipped in batches to the respective laboratories at various times depending on when they were manufactured. Once water conditioning was complete, specimens were returned to NREL in batches and were wrapped in paper towels and plastic film to prevent them from drying out. Table 8 provides information on the dates and total times that the various specimen archetypes were soaked at FAU and PNNL. When received, the specimens were cleaned and stored in a large cold-water tank filled with tap water to maintain saturation until mechanical testing (Figure 18). Immediately before mechanical testing, the specimens were removed from the tank and disassembled, and final mass measurements were taken to compare with those prior to saltwater conditioning.

Table 8. A Summary of the Soaking Dates and Times of Every Specimen Archetype

Specimen Type	Conditioning Location	Start Date	End Date	Total Conditioning Time (days)
T-Bolt	FAU	12-03-2019	12-17-2020	380
	PNNL	12-10-2019	05-25-2021	527
DEI	FAU	02-19-2020	01-06-2021	322
	PNNL	02-09-2021	05-25-2021	105
CCLS	FAU	05-18-2020	12-17-2020	213
	PNNL	02-09-2021	05-27-2021	107
MMLS	FAU	05-18-2020	12-17-2021	213
	PNNL	02-09-2021	05-27-2021	107
SBS	FAU	05-18-2020	12-17-2020	213
	PNNL	02-09-2021	05-27-2021	107
OBS	FAU	05-18-2020	01-04-2021	231
	PNNL	02-09-2021	05-27-2021	107

Figure 18. Cold-water storage tank used to maintain saturation conditions of specimens prior to mechanical testing

3.2 T-Bolt Specimens

Mechanical characterization of the T-bolt specimens was conducted on the 500-kN load frame at NREL's Structural Technology Laboratory. Approximately half of the specimens were tested under static loading and half were tested with fatigue loading. A bespoke fixture was used to attach the specimens between the load frame's base and hydraulic actuator (Figure 19). For the T-bolt connections themselves, Aermet 100 (a high-strength steel superalloy) threaded studs were used with 4340 steel barrel nuts and grade 2H nuts. This was to ensure failure of the

composite specimens before failure of any of the metal components. To promote good alignment of the two T-bolts used in each specimen, a fixture was used to ensure consistent positioning of the barrel nuts relative to the mold surfaces of the specimens (Figure 20). The actuator and base plate of the load frame were also measured using a laser tracker to verify acceptable alignment of the loading path.

Figure 19. The fixture used to connect the T-bolt specimens to the 500-kN load frame

Figure 20. A T-bolt specimen being loaded into the test fixture using the alignment fixture

For static testing, the T-bolts of the specimens were initially torqued to 360 lbf·ft (490 N·m). Later it was found that the resulting preload from this torque was sufficient to fail some of the more severely degraded specimens. Therefore, some of the static tests were conducted with T-bolts torqued to only 100 lbf·ft (135 N·m). Static strength results should have been largely unaffected by this, since full separation of the fixture and specimen were observed before failure, even at the higher bolt preload. All specimens were set up with at least two foil or fiber optic strain gauges to the top and side of one through-hole (Figure 5). Some specimens were instrumented with both foil and fiber optic strain gauges on opposite faces to measure the specimen alignment when loading. All static specimens were loaded to failure at a rate of 2 mm/min. Bearing stresses (σ_B) and tensile stresses (σ_T) were calculated using Eq. 1 and Eq. 2, respectively, where F is the applied load, D_{th} is the measured through-hole diameter, t is the measured specimen thickness, and w is the measured specimen width:

$$\sigma_B = {}^{F}/_{D_{th}t} \tag{1}$$

$$\sigma_T = {}^{F}/_{(w - D_{th})t} \tag{2}$$

For the fatigue testing of the T-bolt specimens, constant amplitude tension-tension loading was applied. To provide valid comparisons of the matrix materials and water conditioning states, the majority of the specimens were tested at the same tensile stress levels. Through some preliminary tests, this was determined to be $\sigma_{T,max} = 130$ megapascals (MPa). All tests were

conducted with $\frac{\sigma_{T,min}}{\sigma_{T,max}} = 0.1$. To prevent repeated separation between the specimens and the test fixture under loading (lash), all T-bolts were torqued to 225 lbf·ft (305 N·m). Foil gauges and fiber optic gauges were located in the same positions as for static testing. Peak-valley strains and displacements were calculated for every fatigue cycle to failure. Additionally, thermocouples were bonded to every specimen in the locations of highest stresses to monitor the stress-induced heating of the specimens (Figure 21). Testing speeds were varied based on these measurements to ensure that specimen temperatures did not exceed 10 °C above ambient. Typically, loading rates ranged from 1 to 4 hertz (Hz).

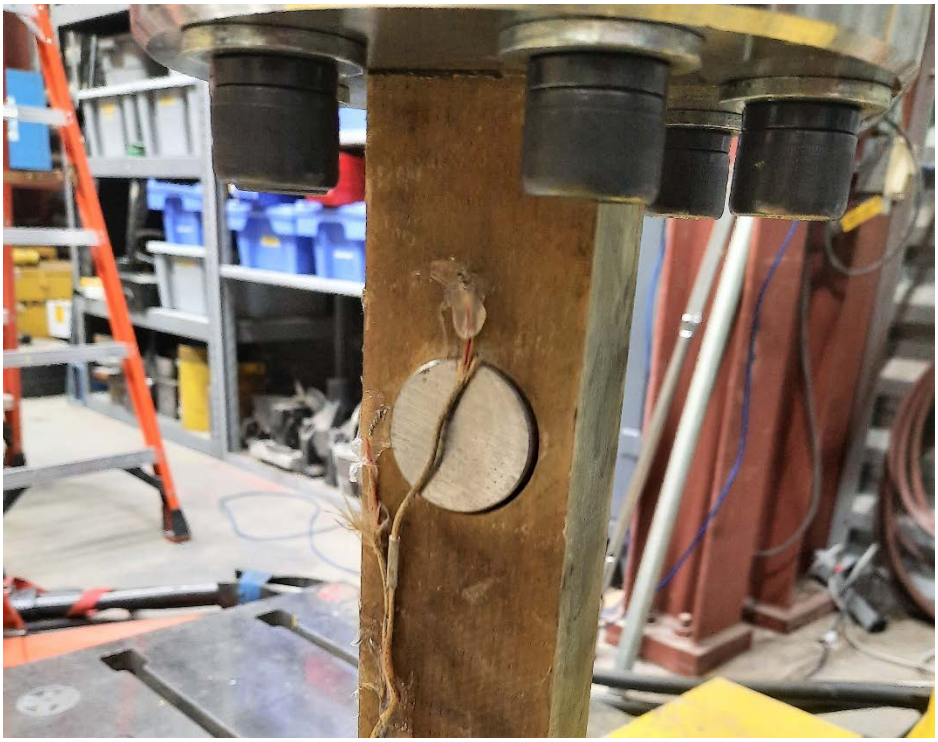

Figure 21. Thermocouples bonded to a T-bolt specimen for fatigue testing

3.3 Double-Ended-Insert Specimens

3.4 Load Frame Testing

Primary testing of the DEI specimens was conducted on the 500-kN load frame. The same cylindrical test fixtures were used to connect the specimens to the load frame (Figure 19). M20 Aermet 100 threaded studs and grade 2H nuts were used to connect the DEI specimens to the test fixture and were torqued to 360 lbf·ft (490 N·m). No other alignment procedures were used to install the specimens beyond the initial manufacturing and bonding of the steel inserts.

All specimens were tested under static loading conditions at 1 mm/min. Load and actuator displacement data were recorded during testing. No strain measurements were taken because all the critical deformations and subsequent failures were occurring beneath the surface of the composite laminates. Adhesive shear stresses (τ_{DEI}) were calculated using Eq. 3, where F is the applied force, D_{insert} is the measured diameter of the steel inserts, and L_{insert} is the embedded

length of the steel inserts. Figure 22 shows a DEI specimen set up in the load frame prior to testing.

$$\tau_{DEI} = {}^{F\pi D_{insert}}/_{L_{insert}} \quad (3)$$

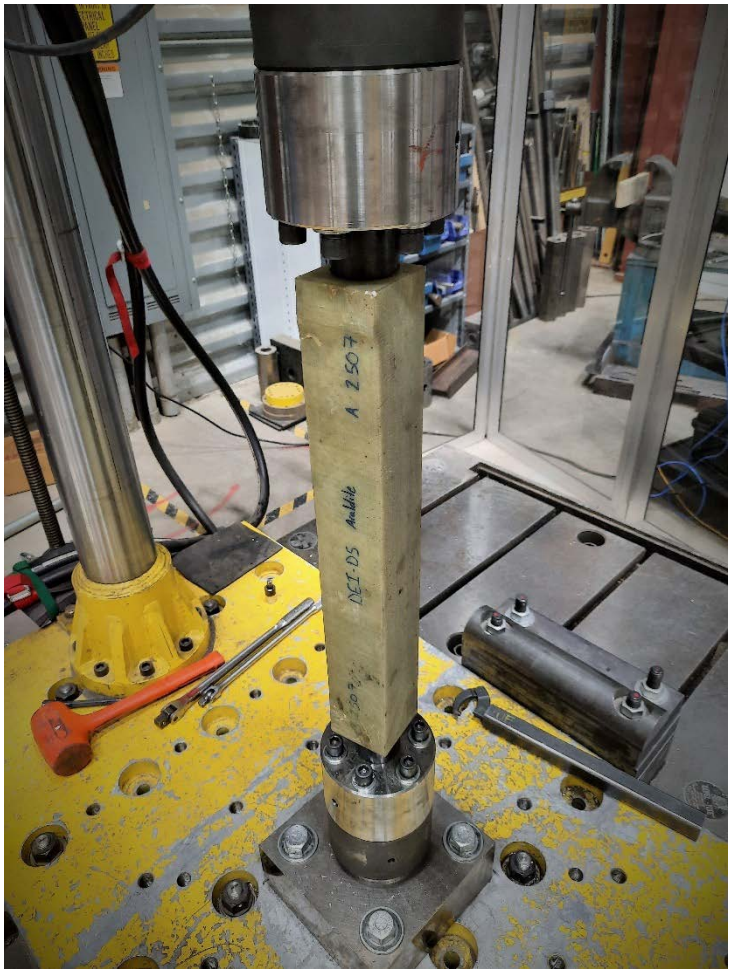

Figure 22. A DEI specimen set up in the load frame prior to testing to failure

3.4.1 Benchtop Testing

Naturally, the load frame testing of the DEI specimens resulted in the failure of only one end of each specimen. Therefore, this was used as an opportunity to develop an alternative benchtop test method to characterize the intact ends of the DEI specimens. It is understood that most marine energy developers do not have the budget for or access to national-lab-quality facilities. Therefore, the remaining ends of the DEI specimens were used to develop a low-cost procedure for performing similar testing that is much more in line with the budgets and expertise of marine energy system developers. The test setup was developed to apply controlled and consistent loads in alignment with the bonded inserts. Figure 23 outlines the test setup used. Tensile forces were applied by an Enerpac Holl-O-Cylinder 10,000 pounds per square inch (psi), 60-ton hydraulic tensioner with a Power Team Quarter Horse hydraulic pump to control the tensioner remotely. Loads from the tensioner were transferred to the DEI specimens via various 4140 steel spacers

and a length of class 12.9 steel M20 threaded rod and were measured using a Transducer Techniques LWO 190-kilopound (kip) and LWO 60-kip load washers. Spherical washers were used to ensure good alignment between the tensioner and specimen and evenly distributed contact on the load washer. For safety, the remote control of the hydraulic pressure supplied to the tensioner allowed the operator to control the system behind a polycarbonate screen.

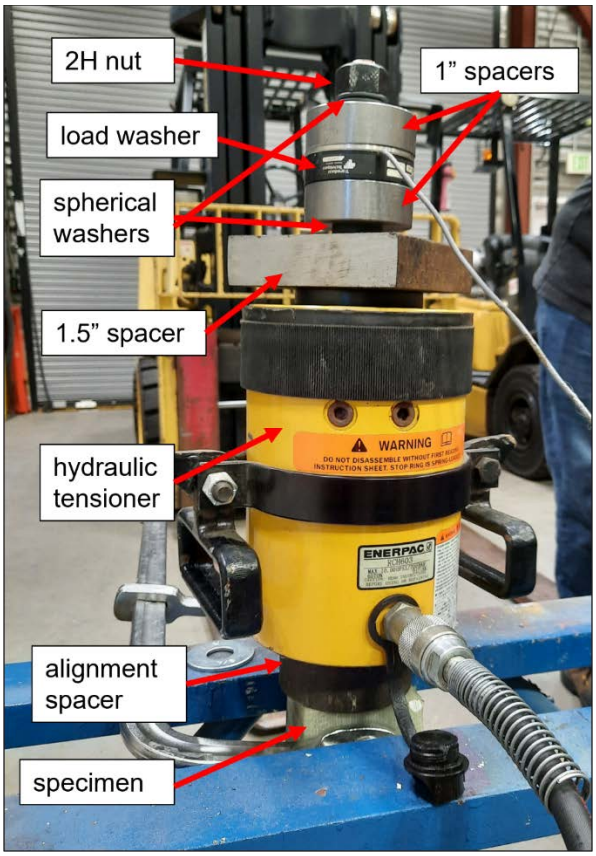

Figure 23. A diagram of the setup used to perform the benchtop static testing of the remaining DEI specimens

Only load data were acquired for this batch of testing. The ultimate shear strength data were not intended to be directly compared with the load frame strength data due to different boundary conditions and conditioned specimens that had been drying out in ambient conditions since they were tested in the load frame previously.

3.5 Lap Shear Specimens

All of the CCLS and MMLS lap shear specimens were tested on an MTS 100-kN load frame. All specimens were tested under static loading conditions, and testing was conducted following ASTM D1003-10 and ASTM D3163-01 standard test methods. Prior to testing, fiberglass and steel end tabs were bonded to the CCLS and MMLS specimens, respectively, with fast-curing epoxy adhesive (Figure 24). This was to ensure uniform axial loading of the specimens and to minimize out-of-plane loading of the bondlines due to misalignments. All specimens were loaded at a rate of 1.3 mm/min. Actuator displacement and force data were acquired during testing, and ultimate shear stresses (τ_{LS}) were calculated using Eq. 4 where l_{LS} is the measured

bondline length and w_{LS} is the measured bondline width for each specimen. Failure modes were observed and documented (adhesive/cohesive). Figure 25 shows a specimen clamped in the load frame prior to loading.

$$\tau_{LS} = {}^{F}/_{l_{LS}w_{LS}} \tag{4}$$

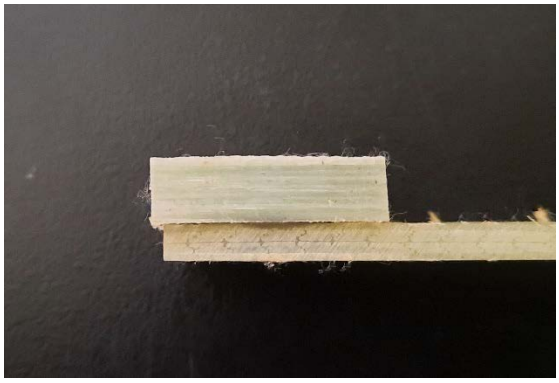

Figure 24. A fiberglass end tab bonded to a CCLS specimen to ensure good alignment in the load frame

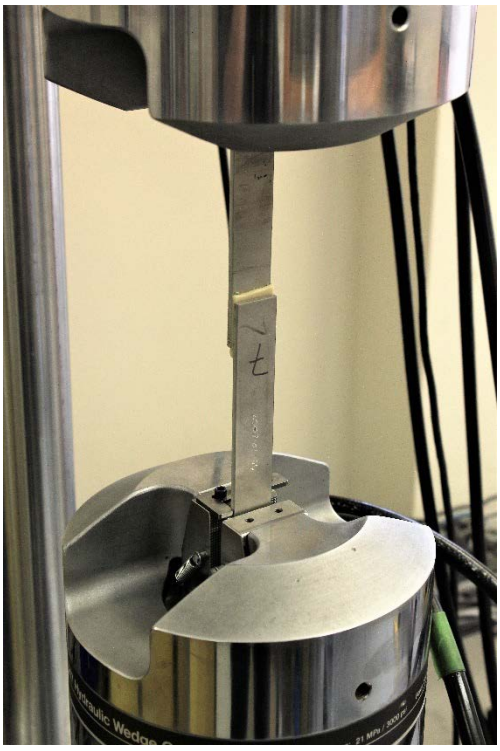

Figure 25. An MMLS specimen clamped in the load frame prior to testing

3.6 Beam Shear Specimens

Both the SBS and OBS specimens were tested in the same MTS 100-kN load frame by generally following ASTM D2344 Standard Test Method for Short-Beam Strength of Polymer Matrix Composite Materials. The SBS specimens were tested on a three-point bending fixture with 3-

mm-diameter support bars and a 6-mm-diameter loading nose (Figure 26). For initial testing, the span between the supports was varied between 50 and 75 mm with the intent of encouraging shear failure between the composite and the adhesive, rather than tension/compression failures of the outer composite layers. From the initial experimentation it was determined that a span of 63.5 mm (2.5 in.) was optimal for shear failures. The majority of the SBS specimens were tested at this span. For the SBS specimens with three composite layers, G10 support and load pads were bonded to the specimens (Figure 27) to prevent failures at the supports or load introduction point. All specimens were loaded to failure at a rate of 0.8 mm/min.

Figure 26. An SBS specimen prepared in the three-point bend fixture before loading to failure

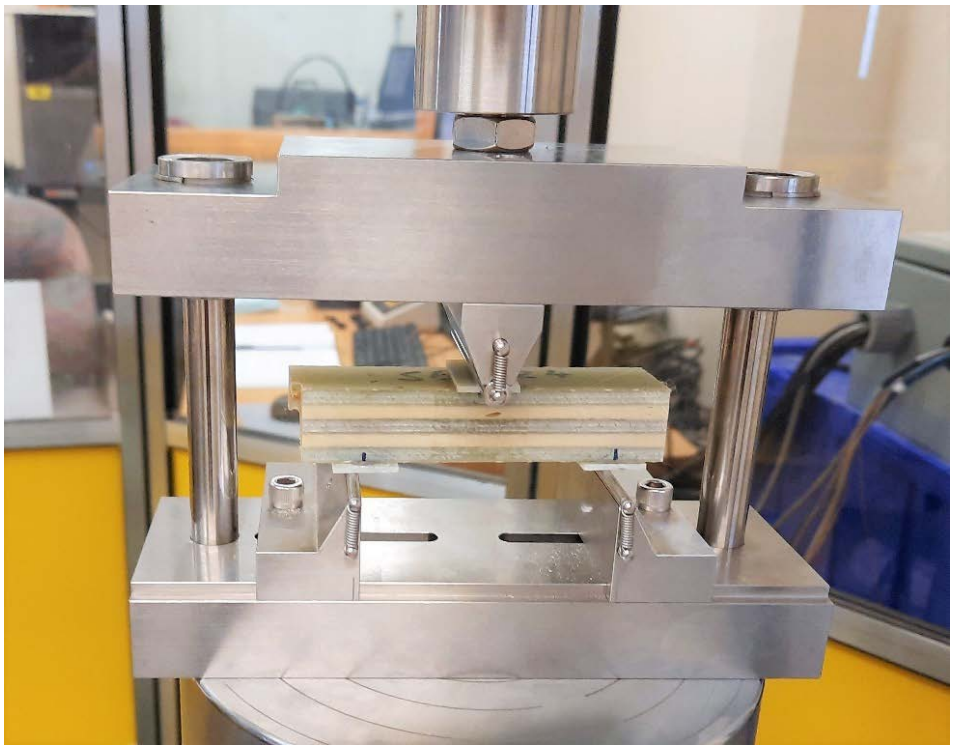

Figure 27. An SBS specimen with three composite layers in the three-point bend fixture with G10 support and load tabs

The OBS specimens were tested on a much larger three-point bend fixture (Figure 28), which is commonly used for composite beam test methods (Murdy, Hughes, and Barnes 2022), such as ASTM C393 Standard Test Method for Core Shear Properties of Sandwich Constructions by Beam Flexure. Like the SBS setup, the support spans for the OBS specimens were set to encourage shear failures of the adhesive layers. The support span was set at 230 mm for all tests. Support and load pads consisted of 25 × 75-mm, freely rotating blocks, with a layer of 3-mm-thick 60A durometer rubber on top to reduce stress concentrations at the load introduction points. All specimens were loaded to failure at a rate of 2.5 mm/min.

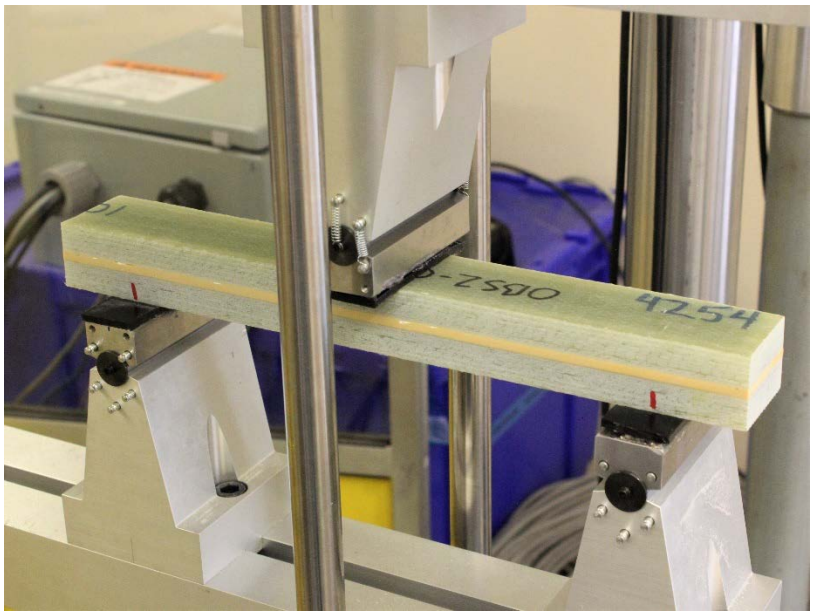

Figure 28. An OBS specimen prepared in the large three-point bend fixture before loading to failure

Axial and shear stress distributions ($\sigma_{xx}(i)$ and $\sigma_{xz}(i)$) were calculated using Eqs. 5 through 8. First, the applied bending moment (M) was determined using the applied load (P) and the distance between the supports (S). The overall sectional stiffness (EI) of the SBS and OBS specimens was determined using Eq. 6, where E_C and E_A are assumed constituent material stiffnesses from manufacturers' data sheets (Table 9) and I_C and I_A are the calculated second moment of areas for the composite and adhesive layers, respectively. This was then used to calculate $\sigma_{xx}(i)$ using Eq. 7, where z_i is the distance from the centroid (the center of the beam cross section) and E_i is the modulus of the constituent material at that specific location in the beam cross section. Finally, $\sigma_{xz}(i)$ was calculated using Eq. 8 as being proportional to the integral of the axial stress distribution. The ultimate adhesive shear strengths ($\tau_{xz,ult}$) were determined to be the average shear stress across the entire adhesive layer. It is assumed that the calculated shear stresses should be largely unaffected by estimated values for composite and adhesive moduli, since they are on different orders of magnitude.

$$M = {PS}/{4} \tag{5}$$

$$EI = E_C I_C + E_A I_A \tag{6}$$

$$\sigma_{xx}(z) = {ME_i z_i}/{EI} \tag{7}$$

$$\sigma_{xy}(z) = \frac{-2}{S}\int_{-z}^{z} \sigma_{xx}(z)\, dz \tag{8}$$

Table 9. A Summary of the Composite and Adhesive Moduli Used To Calculate Axial and Shear Stress Distributions for the SBS and OBS Specimens

Constituent Material	Modulus (gigapascals [GPa])
Quadriaxial fiberglass composite	23.2
Araldite 2015 Adhesive	2.0
Plexus MA560-1 Adhesive	0.3

4 Results

5 Water Absorption

The masses of all specimens returned from PNNL and FAU were recorded prior to mechanical characterization. Before weighing, the specimens were disassembled and thoroughly cleaned of any corrosion from included metal hardware and algae growth on their surfaces.

First, observations of the T-bolt specimens indicated severe corrosion of the hardware that was attached to the specimens, which was attributed to the low-carbon steel used for the compression plates. Some of the specimens had extensive amounts of iron oxide coating their fiberglass composite surfaces (Figure 29). Also noted was that the wired fiber optic gauges that were bonded to some specimens had either completely failed or their connectors were too corroded to be usable. Figure 30 shows the percentage changes in mass of the T-bolt specimens. The Hexion specimens from FAU absorbed substantially more water that the Hexion specimens conditioned at PNNL. This was expected, because the specimens at FAU were conditioned at an elevated temperature, whereas the ones at PNNL were conditioned in water at ambient temperature. Moisture diffusion coefficients in polymers generally increase with temperature (the Arrhenius law). The Derakane specimens, however, absorbed similar amounts of moisture at FAU and PNNL. The variations between specimens received from PNNL were much larger. This may have been caused by substantial amounts of corrosion on the surfaces of the specimens that could not be removed.

Figure 29. Extensive amounts of corrosion (iron oxide) stuck to the surface of T-bolt specimens with broken fiber optic gauges attached

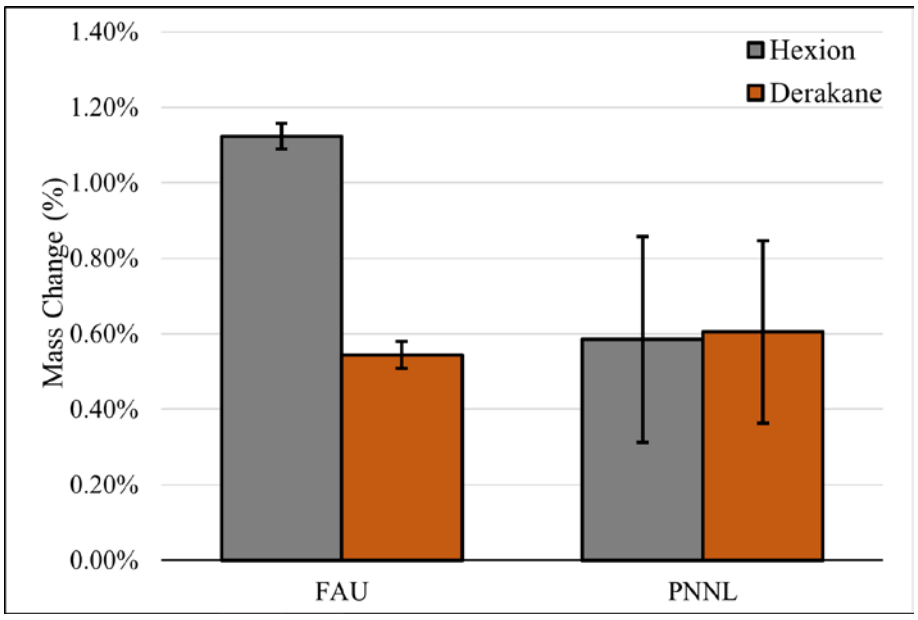

Figure 30. A comparison of percentage mass change of T-bolt specimens from FAU and PNNL (error bars represent standard deviation)

Figure 31 shows the percentage mass changes of the DEI specimens that were conditioned at PNNL and FAU based on their composite matrix materials and the adhesives used to bond their steel threaded inserts. These results show opposite trends to the T-bolt specimens described above. In this case, the specimens with the Derakane matrix apparently absorbed more water than their Hexion counterparts. However, it should be noted that the number of specimens used to produce this data set was limited to only two or three per test condition, which may result in significant uncertainties. Discoloration and streaking were also observed on the surfaces of some of the Hexion specimens conditioned at FAU (Figure 32 [left]) as well as corrosion of some of the 316 steel inserts (Figure 32 [right]). Interestingly, the corrosion of these inserts was only present on the DEI specimens with 316 steel inserts that had been conditioned at PNNL. The specimens conditioned at FAU did not exhibit the same phenomena.

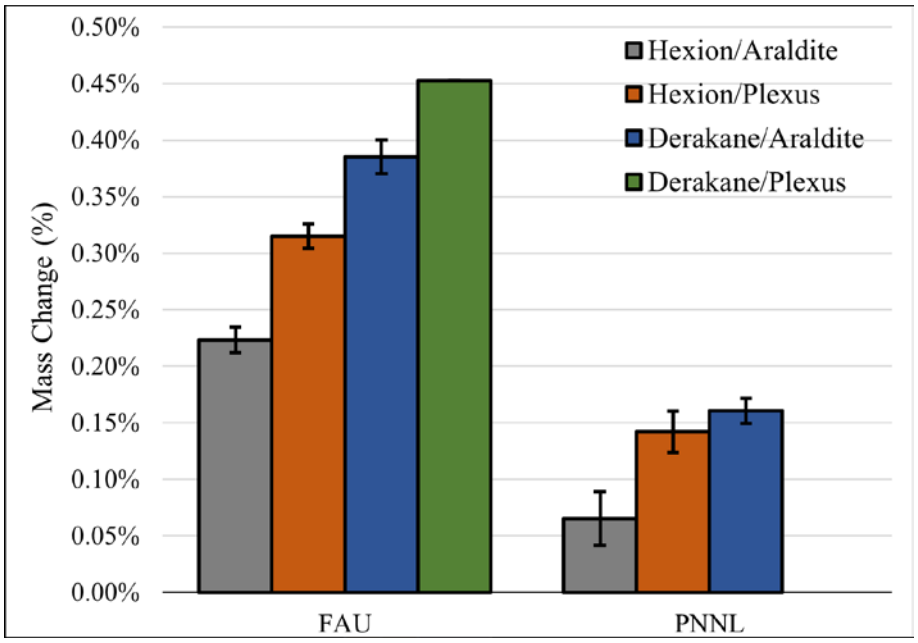

Figure 31. A comparison of the percentage mass changes of the DEI specimens conditioned at FAU and PNNL based on their composite matrix materials and adhesives (error bars represent standard deviation)

Figure 32. (left) Discoloration and streaking on the surface of a Hexion DEI specimen conditioned at FAU and (right) corrosion observed on a 316 steel insert of a DEI specimen conditioned at PNNL

Figure 33 and Figure 34 show the mass change results for the MMLS and CCLS specimens, respectively. Despite only a very small proportion of the MMLS specimens being polymeric, their changes in mass were still measurable. Specimens conditioned at FAU gained the most mass when compared with those conditioned at PNNL. The MMLS specimens made with the 316 steel conditioned at PNNL lost a significant amount of weight, which was likely caused by the corrosion observed around the adhesive bondlines, similar to the DEI specimen shown in Figure 32.

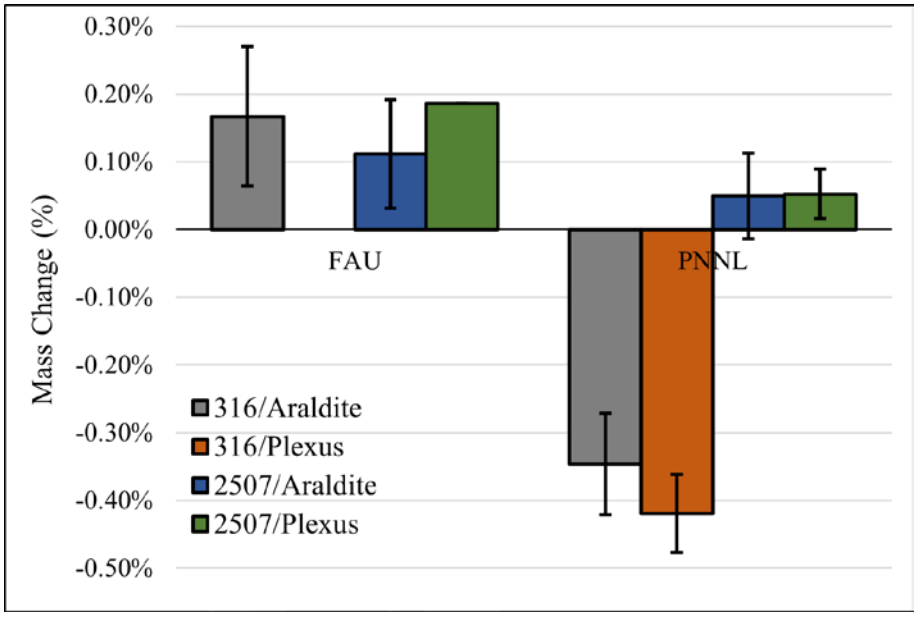

Figure 33. Mass change results for the MMLS specimens conditioned at FAU and PNNL based on the type of steels and adhesives used in their construction (note that the 316/Plexus specimens from FAU were lost in transit; error bars represent standard deviation)

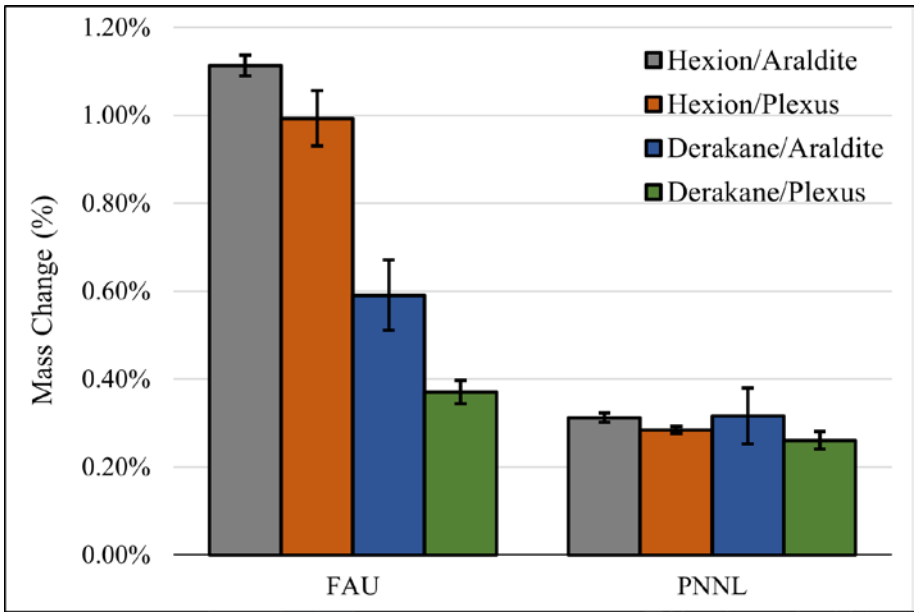

Figure 34. Mass change results for the CCLS specimens conditioned at FAU and PNNL based on the composite matrix materials and adhesives used in their construction (error bars represent standard deviation)

The mass changes of the CCLS specimens are more comparable to the T-bolt specimens. The specimens with the Hexion matrix conditioned at FAU gained the most mass in comparison to the other material combinations. Similar discoloration and streaking were observed on the surfaces of the Hexion specimens conditioned at FAU. Like the other composite specimens, significantly less mass uptake was observed for the specimens conditioned at PNNL, due to the lower conditioning temperatures.

Figure 35 and Figure 36 show the final mass change results for the SBS and OBS specimens, respectively. Again, the differences in mass change between the specimens at FAU and PNNL are significant due to the differences in conditioning temperatures. Another notable observation common with both the SBS and OBS specimens from FAU was the effect of the adhesive used to bond the composite layers. Those bonded with the Araldite epoxy adhesive gained significantly more mass than those bonded with the Plexus methacrylate adhesive. It was not expected that the adhesive would have such a significant effect, because only a very small amount of it was exposed on the surface of the specimens. It is possible that other diffusion mechanisms beyond Fickian diffusion were affecting the total water uptake of the specimens.

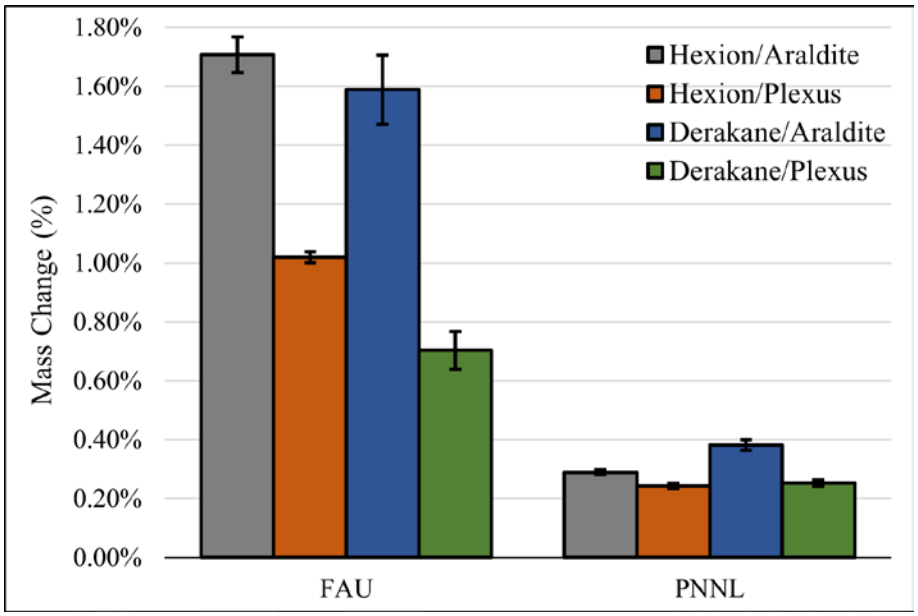

Figure 35. Mass change results for the SBS specimens conditioned at FAU and PNNL based on the composite matrix materials and adhesives used in their construction (error bars represent standard deviation)

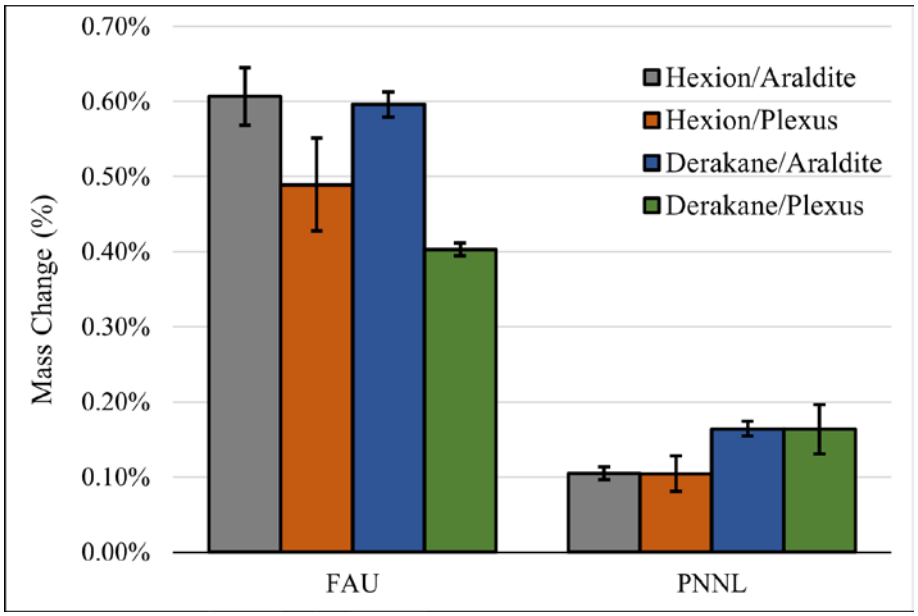

Figure 36. Mass change results for the OBS specimens conditioned at FAU and PNNL based on the composite matrix materials and adhesives used in their construction (error bars represent standard deviation)

5.1 T-Bolt Specimens

Static and fatigue testing were conducted on the T-bolt specimens. As described in Section 2.2, the dimensions of the specimens were modified for fatigue testing because of limitations of the hardware connecting them to the load frame. Consequently, this changed the failure modes

observed during testing. Because of this, the static and fatigue data were analyzed separately rather than combined to produce S-N plots.

5.1.1 Static Testing

Figure 37 shows a comparison of ultimate through-hole bearing strengths for the T-bolt specimens under static loading. Ultimate bearing stress was used as a comparison because all specimens experienced bearing failures at the through-holes (Figure 38). Figure 37 shows that the Derakane matrix specimens exhibited higher ultimate bearing strengths than their Hexion counterparts under all dry and wet conditions. They also showed less significant degradation after being conditioned at PNNL and FAU. As expected, the specimens conditioned at elevated temperatures at FAU showed the largest reductions in strength. Even though the specimens at PNNL were conditioned under ambient ocean conditions for only ~18 months, there are still measurable differences in ultimate bearing strengths from dry to wet. This could be an important realization for real-world deployment of marine energy systems utilizing composite structures.

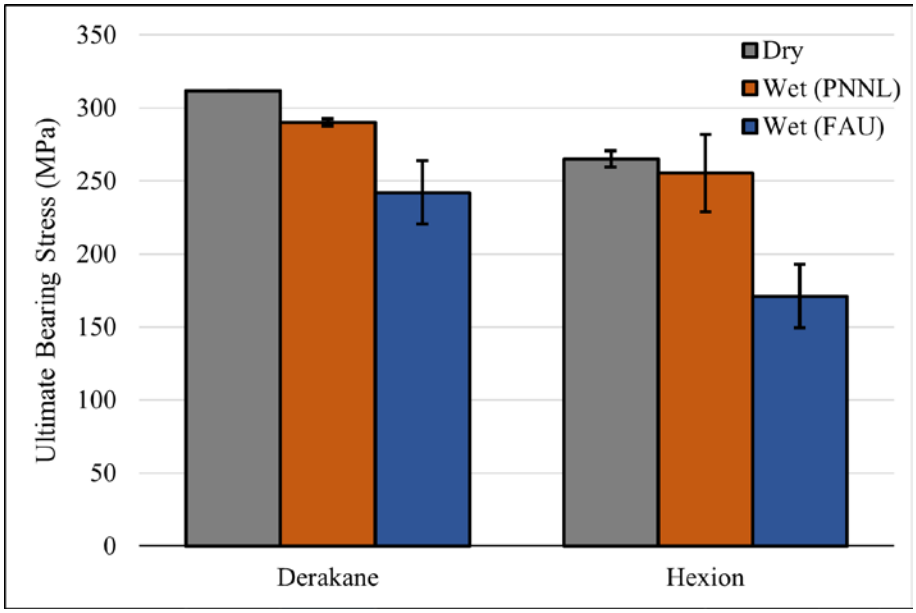

Figure 37. A comparison of ultimate bearing strengths of the T-bolt specimen through-holes under dry and wet conditions (error bars represent standard deviation)

Figure 38. An example of a through-hole bearing failure exhibited by all the T-bolt specimens tested under static loading conditions

Figure 38 shows an example of the through-hole bearing failures of all the T-bolt specimens tested under static loading conditions. Also observed in many of the specimens were lengthwise delamination stemming from the through-holes, which straddled the drill holes in the lengthwise direction. Based on the observed failure modes and the differences in bearing strengths, the results may imply differences in interlaminar properties between the Hexion and Derakane resin systems, although this would need to be confirmed through coupon-scale characterization efforts. It also suggests that the water absorption mechanisms can degrade these properties.

Figure 39 and Figure 40 show representative stress-strain curves from strain measurements taken from the side and top of specimens' through-holes, respectively. It should be noted that all strain gauges were zeroed prior to mounting the specimens in the test fixture and tensioning the T-bolts. Because of this, side and top strains did not all start at zero. Differences in nonzero side strains may also be attributed to misalignment of the T-bolts and the specimens within the load frame. All the measured side strains followed relatively linear trends up to ultimate failure.

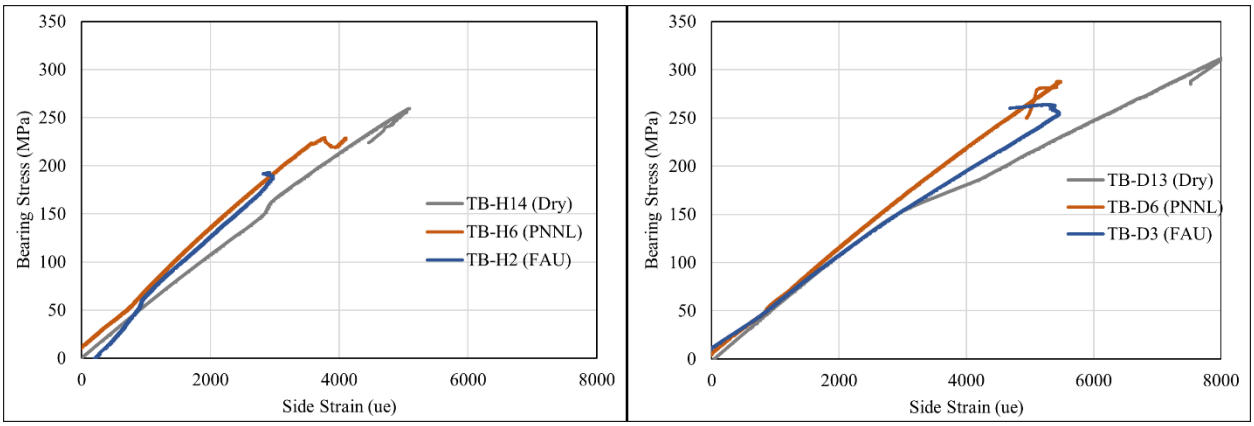

Figure 39. Representative stress-strain curves from T-bolt specimens under each soaking condition with strains taken from the side of the through-holes for (left) Hexion and (right) Derakane specimens

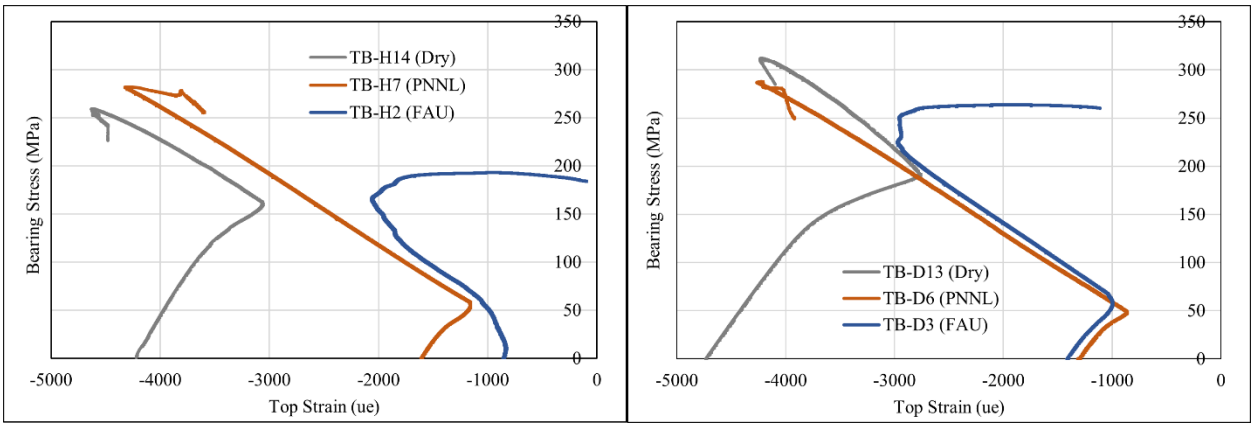

Figure 40. Representative stress-strain curves from T-bolt specimens under each soaking condition with strains taken from the top of the through-holes for (left) Hexion and (right) Derakane specimens

The measured top strains of specimens under no stress were dependent on the torque applied to the T-bolts. For the initial tests, specimens were torqued to 360 lbf·ft (490 N·m), but this was later reduced to 100 lbf·ft (135 N·m). Variability between these strains can be attributed to the inherent uncertainty of using torque wrenches to apply bolt preloads and misalignments of the T-bolts and specimens within the load frame. All of the stress-strain curves first trend toward tensile strains (or reduction in compressive strains) before reaching an inflection point and increasing in compressive strains to ultimate failure. It is assumed that this inflection point indicates separation of the specimen from the fixture due to loss of preload from the T-bolts.

5.1.2 Fatigue Testing

The goal of the fatigue testing of the T-bolt specimens was to conduct constant amplitude, tension-tension tests at the same stress levels for every specimen. Because the specimen dimensions had been modified, data from the static tests could not be used to help determine these stress levels. Preliminary fatigue tests were used to determine a $\sigma_{T,max}$ of 130 MPa (Eq. 2), which would result in fatigue lives ranging from 10^4 to 10^7 cycles to failure depending on the specimen type and conditioning.

Figure 41 shows the average fatigue live of the Hexion and Derakane T-bolt specimens after being subjected to the various water conditions. Note that cycles to failure are plotted on a logarithmic scale for comparison. Generally, two specimens were tested per condition, but only one dry Hexion specimen was tested due to time limitations. Contrary to the static strength results, the dry Hexion specimens exhibited much better fatigue lives than their Derakane counterparts. The number of cycles to failure of the dry Hexion specimens was almost two orders of magnitude greater than the dry Derakane specimens. The specific reason for this is unknown but could be related to the change in failure mechanisms as a result of modifying the dimensions of the specimens. All specimens failed by tensile failure at the through-hole (Figure 42). Tension-tension fatigue testing of the materials at the coupon scale would help facilitate understanding of these large differences in fatigue lives.

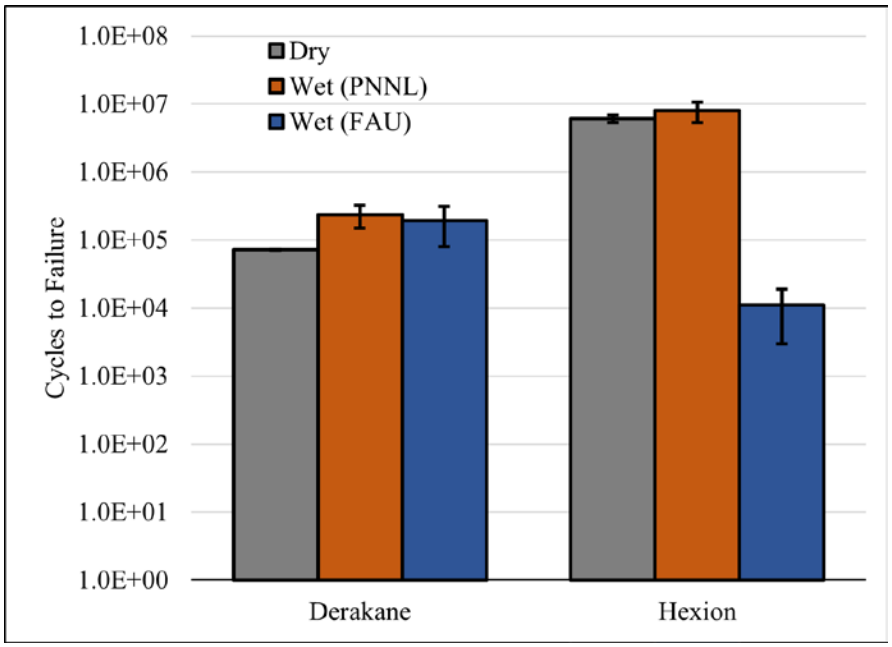

Figure 41. A comparison of fatigue lives for T-bolt specimens under constant-amplitude, tension-tension loading with a maximum tensile stress of 130 MPa for Derakane and Hexion specimens (error bars represent standard deviation)

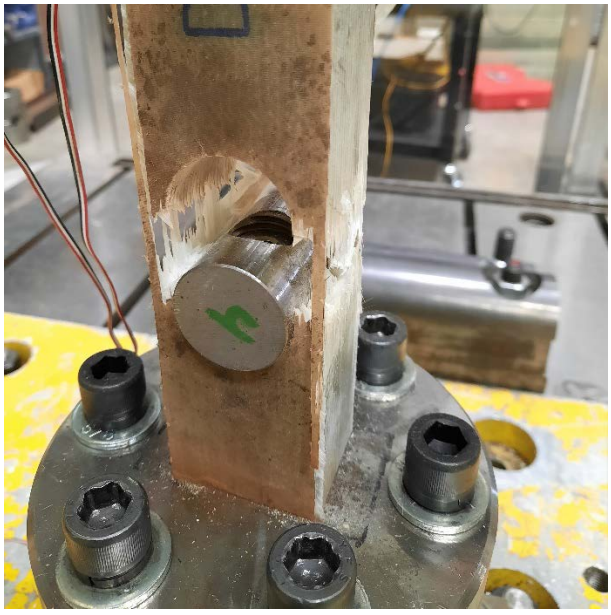

Figure 42. A typical through-hole tensile failure observed for all the T-bolt specimens tested under fatigue loading

The fatigue life of the Hexion specimens was largely unaffected after being subjected to Pacific Ocean water conditions at PNNL. The Hexion specimens conditioned at elevated temperatures at FAU did exhibit severe fatigue life degradation on the order of almost three magnitudes. The Hexion specimens from FAU absorbed significantly more water than any of the other T-bolt specimens. On the other hand, the Derakane specimens exhibited little to no changes at all after being exposed to Pacific Ocean water at PNNL and salt water at elevated temperatures at FAU.

This demonstrates that the Derakane vinyl ester resin system has a strong resistance to marine environments over long periods of time.

Figure 43 shows a comparison of peak-valley displacement trends against life fraction for representative specimens tested under each condition. All specimens demonstrated characteristic trends for stiffnesses of composites under tension-tension fatigue loading. The largest changes in stiffness occurred in the first and final 10% of the specimens' fatigue life.

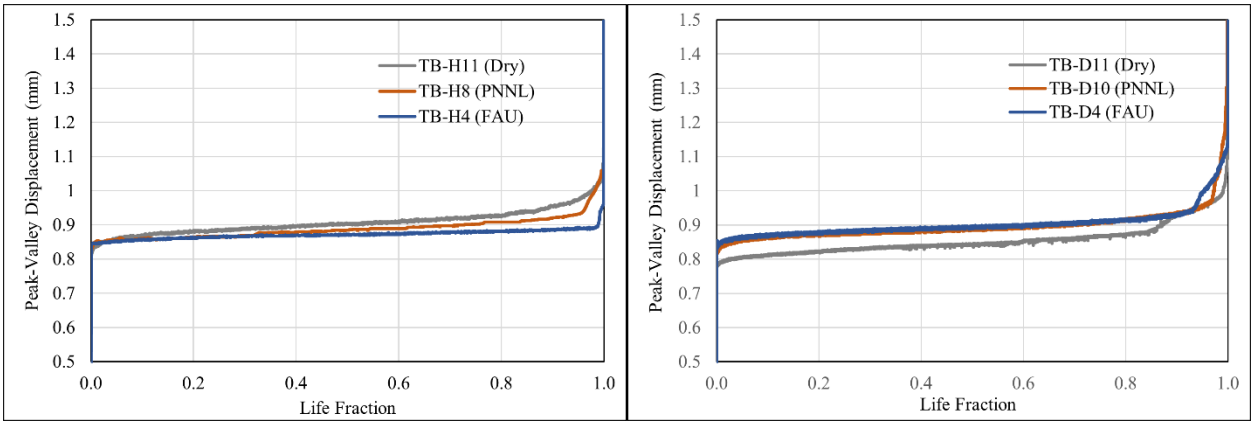

Figure 43. A comparison of peak-valley displacement trends over the fatigue life of representative (left) Hexion and (right) Derakane T-bolt specimens

5.2 Double-Ended-Insert Specimens

5.3 Load Frame Testing

Figure 44 shows a summary of the calculated ultimate adhesive shear strengths of the DEI specimens with the various steels and adhesives used. Overall, the 2507 steel inserts appear to have performed better than the 316 steel inserts and bonded better with the Araldite and Plexus adhesives. The shear strengths of the specimens using the Araldite adhesive do not appear to have experienced much degradation from exposure to saltwater conditions at PNNL and FAU. Significant degradation was not expected because water would have to penetrate a large distance through the adhesive or composite material to have a measurable effect on strength. However, the DEI specimens with Plexus adhesive did show drops in strength after being submerged at FAU and PNNL, despite the specimens at PNNL only being submerged in water for 105 days. On inspection of the failed specimens, moisture was observed deep in the adhesive bondlines (Figure 45).

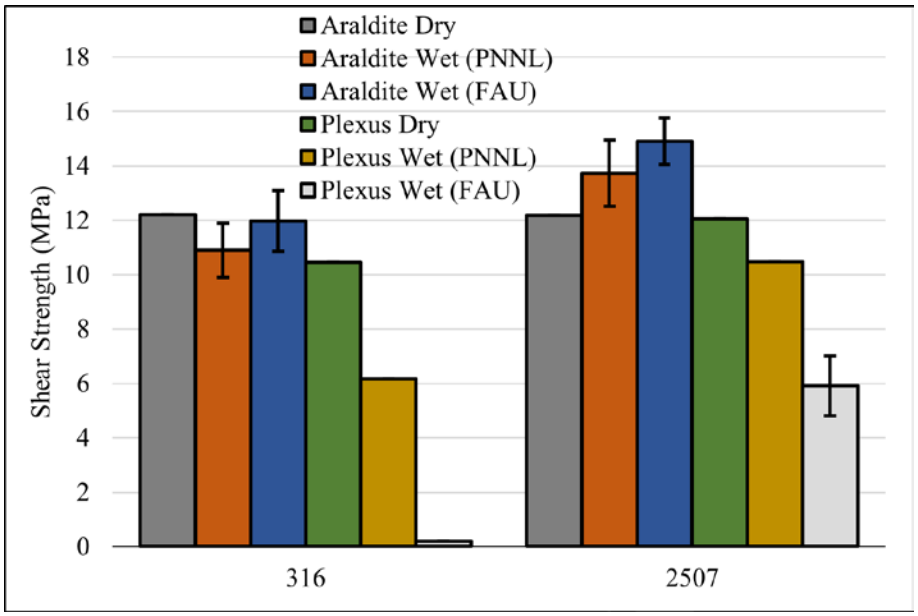

Figure 44. A comparison of ultimate shear strengths for the DEI specimens (error bars represent standard deviation)

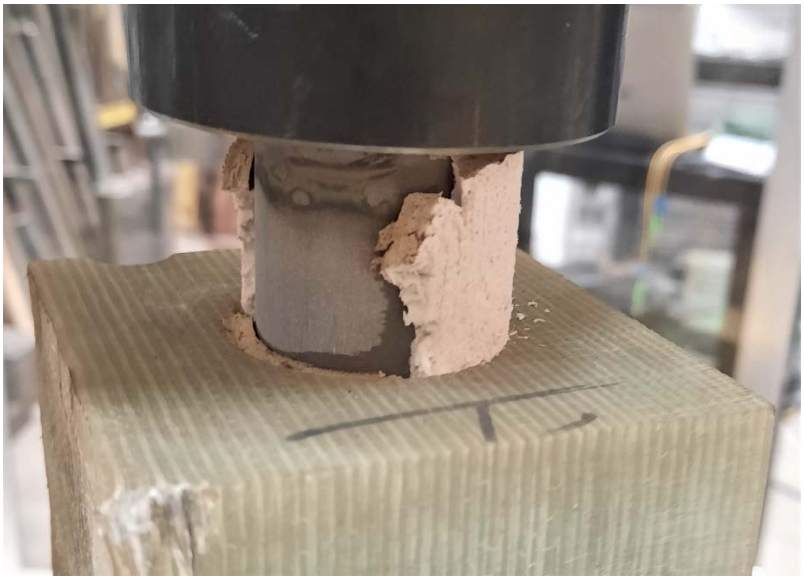

Figure 45. Moisture observed deep in the adhesive bondline of a DEI specimen with Plexus adhesive

Another observation of note was the corrosion of the 316 steel inserts described in Section 4.1; corrosion was only observed on specimens that were conditioned under ambient conditions at PNNL. Upon failure of the specimens, this corrosion was observed deeper than just the surface (Figure 46). The corrosion was present on all DEI specimens with 316 steel inserts conditioned at PNNL. The specific reasons for the localized corrosion are unknown, as is why the specimens conditioned at FAU did not also experience corrosion. Some causes of the corrosion could have been soaking temperature, salinity, microbial life, or adhesive/steel chemical interactions. More investigation is required to understand this phenomenon. Also observed was that the DEI

specimens with Plexus adhesive regularly failed at the composite/adhesive interface rather than the insert/adhesive interface like the Araldite specimens (Figure 47). This indicates that the Plexus adhesive bonded to the metal inserts much better than it bonded to the composite materials.

Figure 46. Corrosion observed in the adhesive bondline of a DEI specimen with 316 steel inserts that was conditioned at PNNL

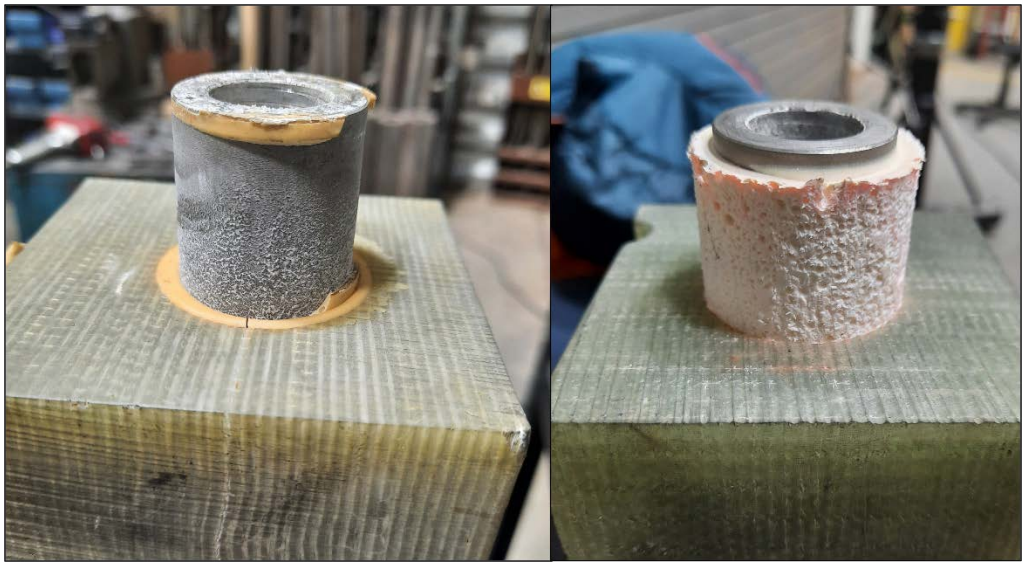

Figure 47. Photographs demonstrating the differences in failure modes observed between the (left) Araldite and (right) Plexus DEI specimens

5.3.1 Benchtop Testing

Initial benchtop testing of the opposite end of failed DEI specimens proved difficult. Initially, only one load washer was used, and the measured loads were sporadic and misleading. Some of the ultimate loads measured well exceeded the ultimate strength of the threaded rod used to pull on the inserts. In subsequent tests, multiple load washers were used in various configurations to compare results and understand their sensitivities to setup and alignment.

Comparisons between the load washers indicated significant variations in measured loads, which was sometimes more than 20% (Figure 48). It is suspected that these differences were due to changes in the alignment of the load washers and the load train between tests. Efforts were made to improve the setup alignment with little to no success. Typically, load washers do not come with the ability to compensate for out-of-plane loads and moments. In the future, this benchtop test method could be improved by implementing better quality load cells into the setup to better account for minor misalignments.

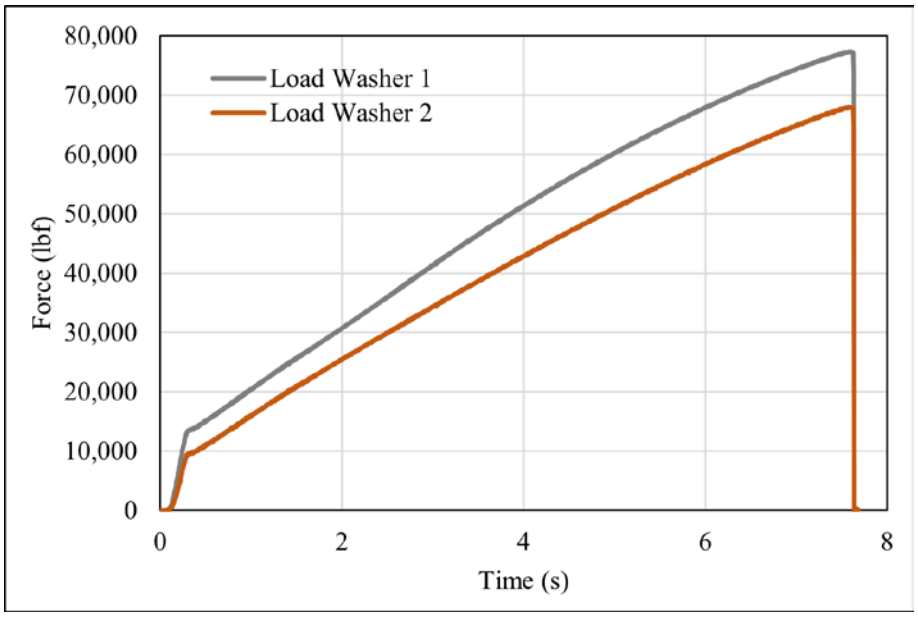

Figure 48. A comparison of measured loads between two load washers for a DEI specimen tested using the benchtop setup

5.4 Lap Shear Specimens

Figure 49 shows a comparison of ultimate shear stresses for the MMLS specimens. Generally, the Plexus specimens outperformed the Araldite specimens, although some test cases were limited due to specimens lost during shipping. The Plexus specimens often demonstrated cohesive failures, whereas the Araldite specimens were all adhesive failures (Figure 50).

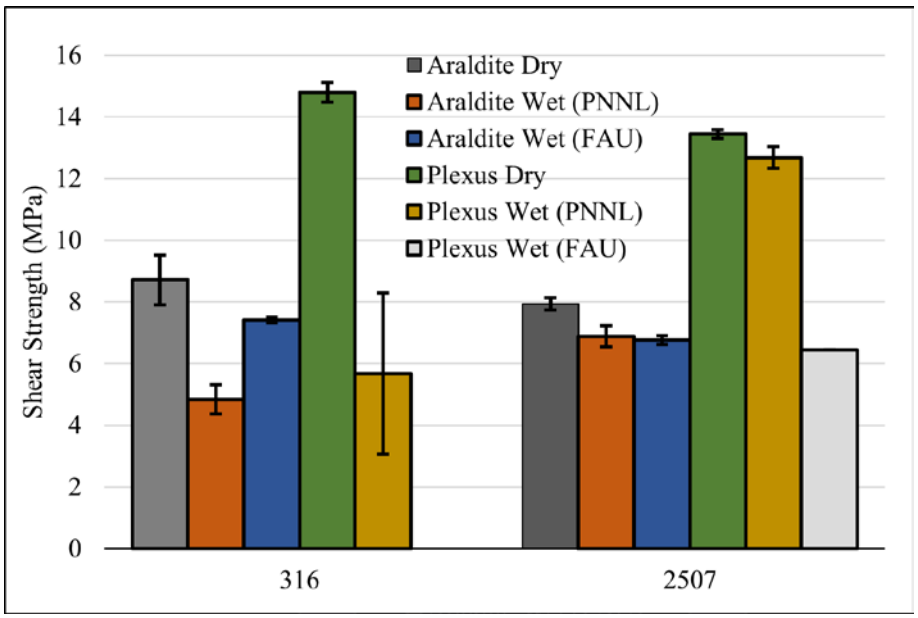

Figure 49. A comparison of ultimate shear strengths for the MMLS specimens (error bars represent standard deviation)

Figure 50. A comparison of failure modes observed in the (left) Araldite and (right) Plexus MMLS specimens

The 316 steel specimens that were subjected to the water conditions at PNNL suffered severe degradation. Like the DEI specimens, corrosion was observed deep in the metal/adhesive interface (Figure 51), despite the short time that they were conditioned in PNNL's tanks. Again, the exact cause of this phenomenon is unknown, and further research is required to understand the interactions among steel, adhesives, soaking temperature, salinity, and microbial life. Some degradation was observed for the 2507 steel specimens but not to the same degree. There appeared to be minimal differences between those conditioned at elevated temperatures at FAU and those conditioned under ambient temperatures at PNNL.

Figure 51. Corrosion observed deep in the bondlines of 316 steel MMLS specimens conditioned at PNNL

Another interesting observation of the Plexus MMLS specimens conditioned at FAU was mixed adhesive/cohesive failures in some instances (Figure 52). They provided a great visualization of how far water had penetrated into the bondlines around the edges and how it degraded the adhesion.

Figure 52. Mixed adhesive/cohesive failure of a Plexus MMLS specimen conditioned at FAU

Figure 53 provides a comparison of ultimate shear strengths for the CCLS specimens. The main failure modes observed were adhesive, aside from some of the Plexus specimens presenting mixed adhesive/cohesive failures for some specimens (Figure 54). Again, the Plexus adhesive

appears to have significantly outperformed the Araldite adhesive. The Plexus specimens conditioned at PNNL exhibited very little degradation, compared to those conditioned at FAU, particularly the Hexion/Plexus combination. The specimens bonded with Araldite showed very little degradation due to conditioning at PNNL or FAU.

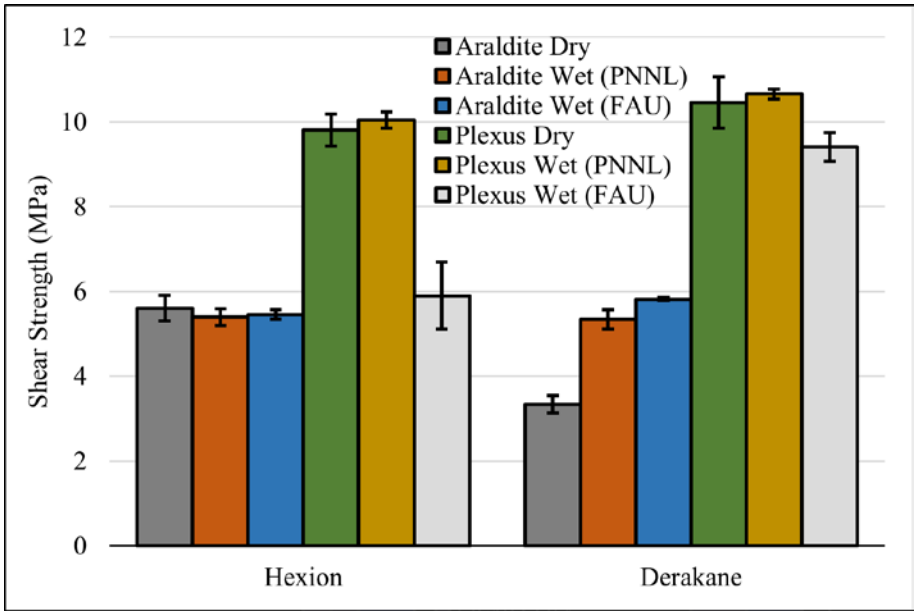

Figure 53. A comparison of shear strengths for the CCLS specimens (error bars represent standard deviation)

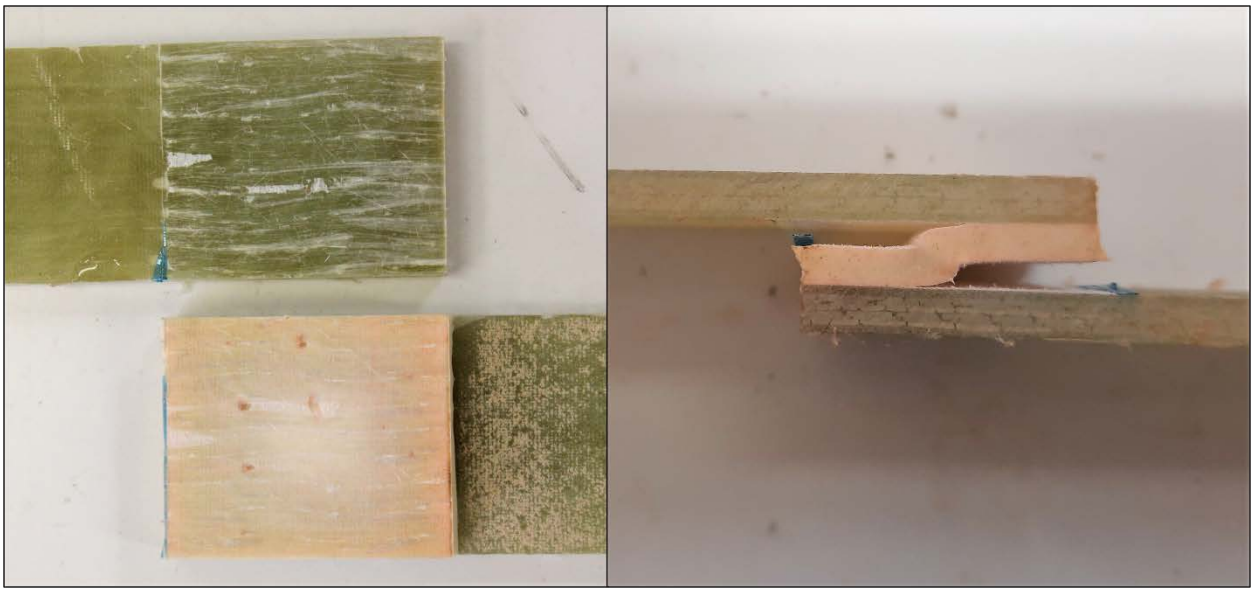

Figure 54. Examples of (left) adhesive and (right) mixed adhesive/cohesive failures exhibited by all the CCLS specimens

5.5 Beam Shear Specimens

Figure 55 and Figure 56 show the calculated ultimate adhesive shear stresses for the two-layer and three-layer SBS specimens, respectively. The results followed very similar trends between the Hexion and Derakane and the number of composite layers. It should be noted that the ultimate shear strengths were significantly higher than those determined by the lap shear tests. The lap shear tests were likely influenced by rotation of the overlap caused by eccentric tensile loads. This could indicate that the short-beam-shear test is more appropriate for the evaluation of thick adhesive bondlines. In this instance, there were little differences between the Araldite and Plexus adhesives under dry conditions. Conditioning the specimens at PNNL had very little influence on the ultimate shear strength of the adhesives. However, the specimens conditioned at FAU exhibited severe strength degradation, but this was not caused by degradation of the adhesives in this case.

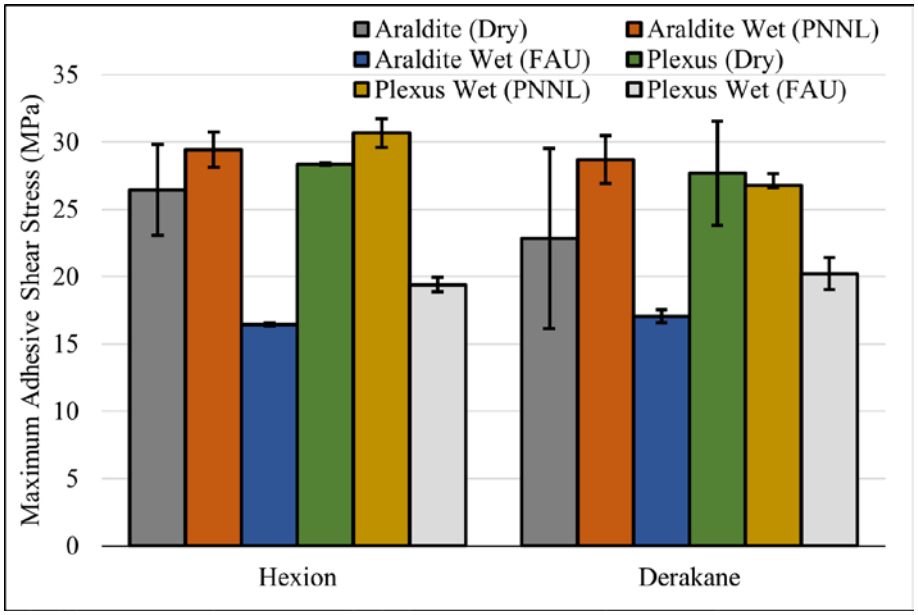

Figure 55. A comparison of calculated ultimate shear stresses for the two-layer SBS specimens (error bars represent standard deviation)

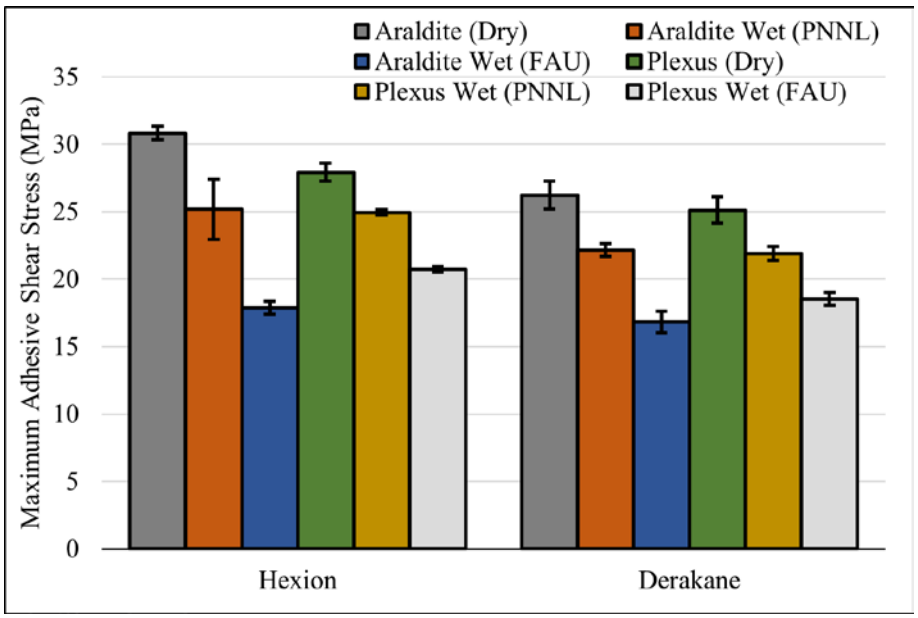

Figure 56. A comparison of calculated ultimate shear stresses for the three-layer SBS specimens (error bars represent standard deviation)

The differences observed between the dry and PNNL specimens when compared with the FAU specimens were due to a fundamental shift in failure modes caused by the water absorption process. The dry and PNNL specimens failed at the adhesive layers as intended due to shear stresses. The Araldite specimens failed through sudden shear failure at the adhesive/composite interfaces, and the Plexus adhesive appeared to yield and stretch along the length of the bondline (Figure 57). On the other hand, the specimens conditioned at FAU did not fail at the adhesive. They generally failed in compression and tension at the outermost composite plies at the load introduction points (Figure 58). The water absorption process degraded the outermost composite plies and caused a significant strength reduction of the specimen as a whole.

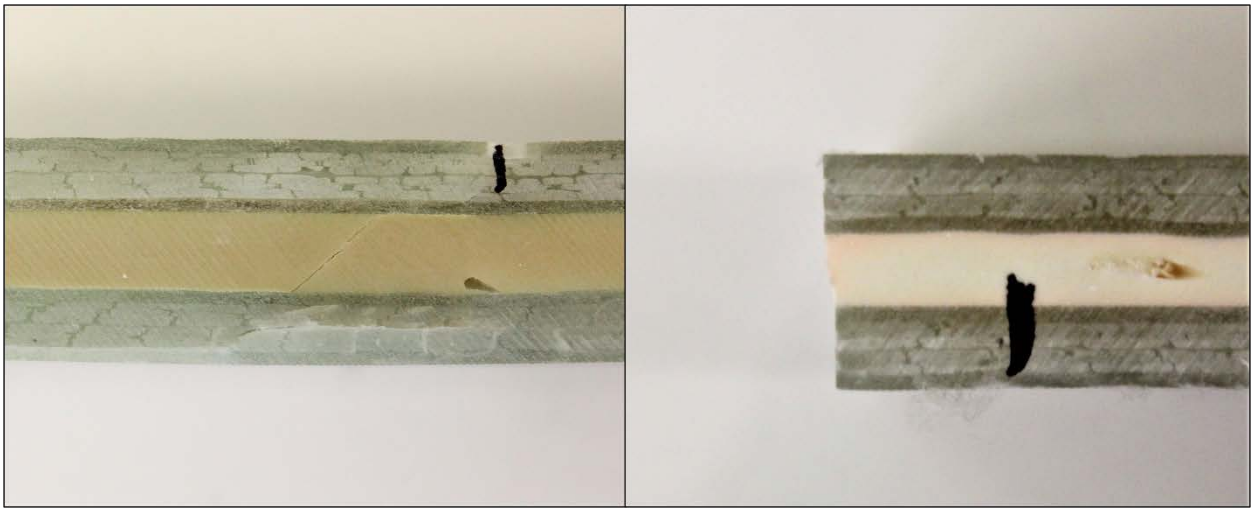

Figure 57. Adhesive shear failure modes observed for the (left) Araldite and (right) Plexus SBS specimens that were dry or conditioned at PNNL

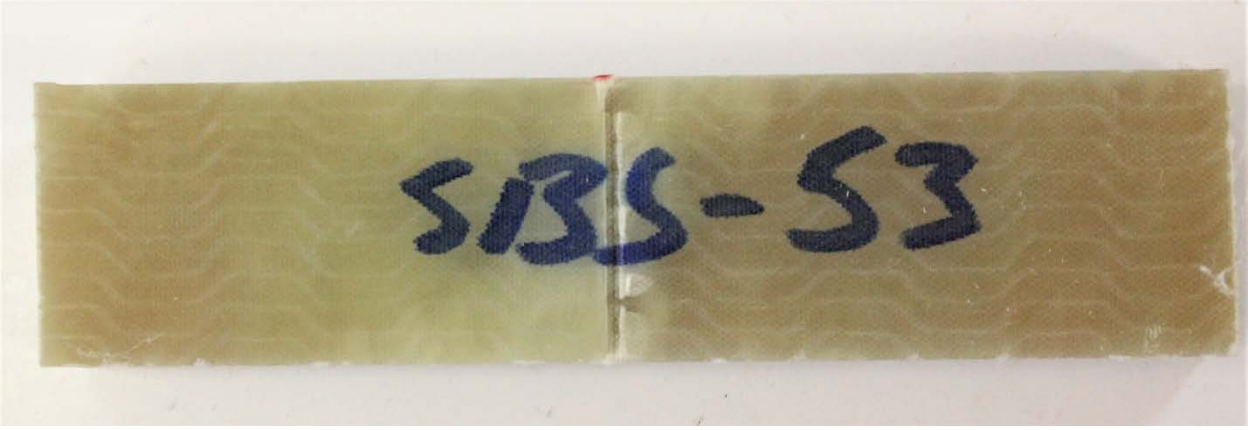

Figure 58. A typical compressive failure observed at the load introduction point of a SBS specimen conditioned at FAU

Figure 59 and Figure 60 show the calculated ultimate adhesive shear stresses for the two-layer and three-layer OBS specimens, respectively. They show comparable ultimate shear strengths to the SBS specimens. Generally, the shear strengths were not significantly affected by the water conditioning at PNNL. However, the results indicate that the Araldite adhesive did not bond to the Derakane matrix composites as well when compared to the Hexion epoxy composite laminates. Again, large drops in strength were observed for the specimens conditioned at FAU due to similar changes in failure mode. The dry specimens and those conditioned at PNNL generally exhibited shear failure of the adhesive by cracking for the Araldite and yielding for the Plexus (Figure 61). The specimens conditioned at FAU all failed by axial compression and crushing at the load introduction point (Figure 62). Overall, this shift in failure modes indicates that severe degradation of composite laminates from water absorption needs to be anticipated and accounted for when designing new test methodologies to ensure the desired failure modes will occur.

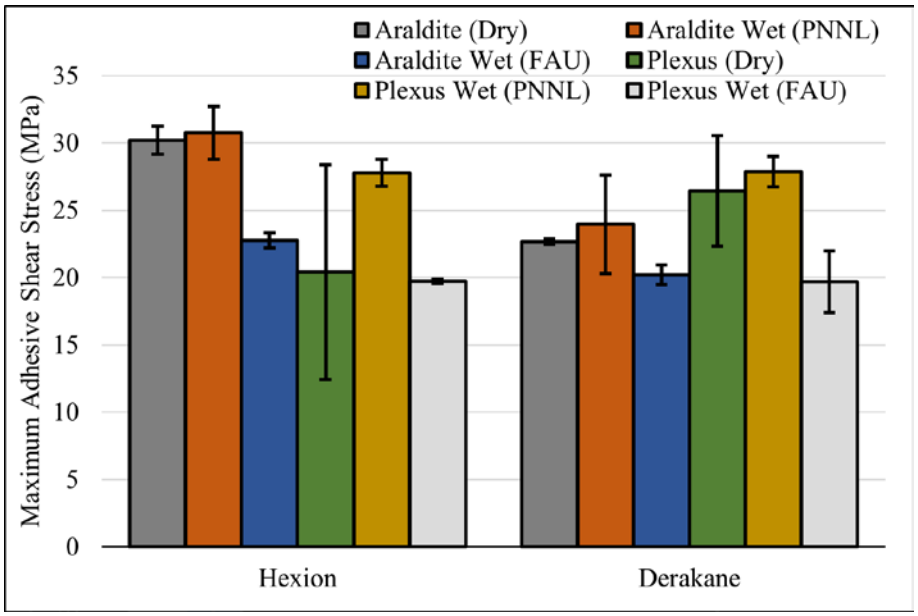

Figure 59. A comparison of calculated ultimate shear stresses for the two-layer OBS specimens (error bars represent standard deviation)

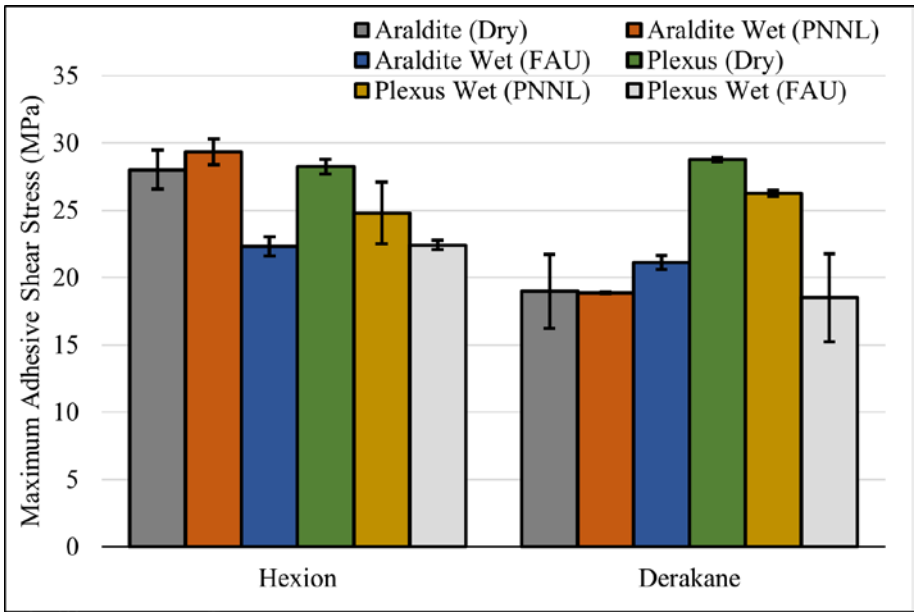

Figure 60. A comparison of calculated ultimate shear stresses for the three-layer OBS specimens (error bars represent standard deviation)

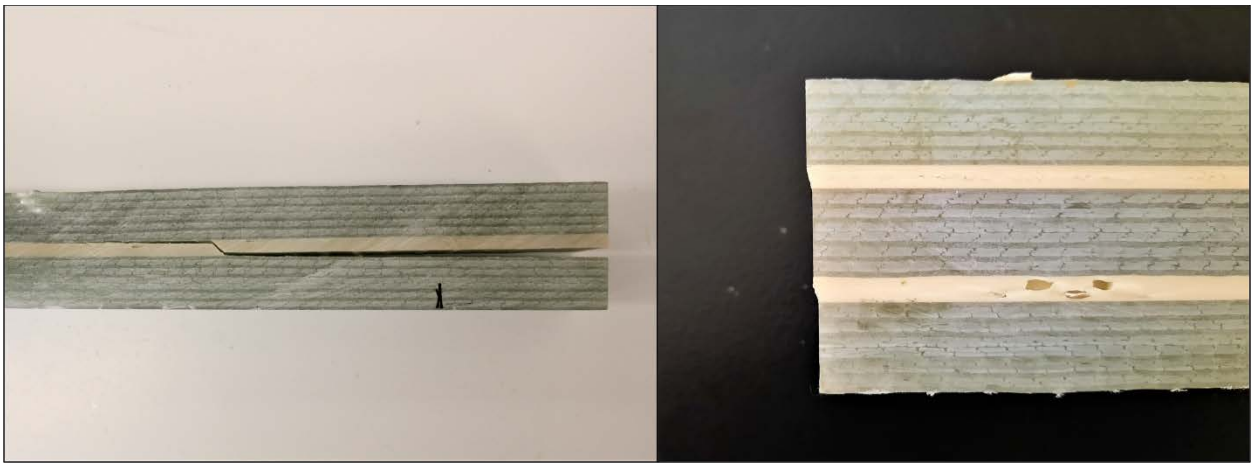

Figure 61. Adhesive shear failure modes observed for the (left) Araldite and (right) Plexus OBS specimens that were dry or conditioned at PNNL

Figure 62. A typical axial compression and crushing failure observed at the load introduction point of a OBS specimen conditioned at FAU

6 Conclusions and Future Work

Over the past 3 years a large, multilaboratory subcomponent structural testing campaign has been conducted to investigate various composite and metal materials and methods for connecting them. Upward of 300 specimens of six different geometries manufactured at MSU and NREL were subjected to saltwater conditioning at FAU and PNNL and then structurally validated by NREL. It was perhaps the largest study of its kind to be performed to date. The goal was to develop appropriate subcomponent test methods to evaluate composite materials, adhesives, metals, and interconnects and understand their interactions when subjected to corrosive seawater environments. Key takeaways from the study are as follows:

- Partial saturation of thick composite specimens (T-bolt specimens), especially at elevated temperatures, can have pronounced effects on static and fatigue strengths.
- Conducting fatigue testing at the subcomponent scale (T-bolt specimens) can be time-consuming and expensive, requiring detailed project planning to ensure like-for-like comparisons.
- Steel inserts embedded deep into composites with adhesive (DEI specimens) are less susceptible to water absorption mechanisms, at least for short conditioning periods.
- Under the right conditions, interactions between 316 steel and adhesives can cause the steel to corrode in bondlines (316 MMLS and DEI specimens at PNNL), even over short periods, and leads to large strength reductions. More investigation is necessary to understand this phenomenon.
- Short-term conditioning of composite-composite adhesive joints had little effect on the strength (CCLS specimens at PNNL), but accelerated aging at elevated temperatures caused severe degradation (CCLS specimens at FAU).
- Thick adhesive beam shear testing showed potential to provide reliable data for evaluating thick adhesive bondlines (SBS and OBS specimens).
- The thick adhesive beam shear specimens were not appropriate for evaluating environmental effects in their current state (SBS and OBS specimens) because greater degradation of the composite layers caused them to fail before the adhesive.
- The results from this project will help marine energy developers make informed material choices and understand the complex requirements for evaluating new materials for use in large marine energy structures.

Based on the key findings outlined above, there is a lot of potential for future work in the proceeding phases of this research. At the beginning of this study, we did not anticipate observing such significant static and fatigue strength differences for partially saturated thick composites. Because of this, it is important to understand how far water actually penetrated into the bulk composites and adhesives. In the future, water penetration depth will be evaluated through the development of finite difference models to simulate the water diffusion process

through multiple materials, which will then be validated by the mass measurements recorded in this study. The resulting finite difference models could be combined with finite-element models to apply water-absorption-induced degradation from coupon-scale characterization data to understand the reductions in strength of thick composite structures.

In this study, the water absorption and structural testing were performed sequentially. In reality, marine energy structures will be subjected to water intrusion and fatigue loading simultaneously. It is important that any potentially synergistic effects are investigated in the future in the form of submerged fatigue testing. This will be particularly difficult since the temperature-accelerated water absorption testing and fatigue loading occurred on very different time frames. Another challenge with coupon fatigue testing will be to understand how acceleration of fatigue test loads, by increasing cyclic test frequencies or simplifying complex variable amplitude operational loads to constant amplitude test loads, can properly represent in-water operational conditions. Good understanding of the water absorption models outlined above will be required to tune soaking temperatures and loading rates for realistic testing. In addition, fatigue degradation models should be used to support this testing.

Another unexpected highlight of this study was the corrosion observed on the 316 steel specimens that were conditioned at PNNL. Further investigation and conditioning at both FAU and PNNL are needed to understand the cause of the corrosion and how similar types of stainless steel, such as 316L, may also be affected.

Finally, future research will continue to investigate other critical design details that may be utilized for marine energy composite structures as the industry grows and will also explore other commonly used composite materials and future materials, such as thermoplastic composites and bio-derived, recyclable resin systems. Ultimately, the goal of this research was to develop subcomponent-scale validation methods for marine energy materials and address barriers and uncertainty currently facing marine energy developers with regard to composite materials, and future research will continue to meet this goal.

References

Ashworth Briggs, Alexander J. E., Zhongyi Y. Zhang, and Hom N. Dhakal. 2014. "Study on T-bolt and pin-loaded bearing strengths and damage accumulation in E-glass/epoxy blade applications." *Journal of Composite Materials* 49(9): 1047–1056. https://doi.org/10.1177/0021998314528825.

Bahri, Abbas, Manouchehr Salehi, and Mehdi Akhlaghi. 2014. "Using a pseudo-functionally graded interlayer in order to improve the static and dynamic behavior of wind turbine blade T-bolt root joints." *Composite Interfaces* 21(8): 749–770. https://doi.org/10.1080/15685543.2014.950162.

Bender, J. J., S. R. Hallett, and E. Lindgaard. 2019. "Investigation of the effect of wrinkle features on wind turbine blade sub-structure strength." *Composite Structures* 218: 39–49. https://doi.org/10.1016/j.compstruct.2019.03.026.

Ennis, Brandon Lee, and Joshua A. Paquette. 2015. *NRT Rotor Structural/Aeroelastic Analysis for the Preliminary Design Review*. Albuquerque, NM: Sandia National Laboratories. SAND2015-9358. https://www.osti.gov/servlets/purl/1225852/.

Hernandez-Sanchez, Bernadette A., Budi Gunawan, James Nicholas, David Miller, George Bonheyo, Scott Hughes, Paul Murdy, and Francisco Presuel-Moreno. 2019. "Developing Materials for Marine Renewable Energy Technologies." Albuquerque, NM: Sandia National Laboratories. SAND2019-13759PE. https://www.osti.gov/servlets/purl/1646251.

Lee, Hak Gu, Min Gyu Kang, and Jisang Park. 2015. "Fatigue failure of a composite wind turbine blade at its root end." *Composite Structures* 133: 878–885. https://doi.org/10.1016/j.compstruct.2015.08.010.

Miller, David A., Daniel D. Samborsky, Mark T. Stoffels, Michael M. Voth, Jake D. Nunemaker, Kai J. Newhouse, and Bernadette A. Hernandez-Sanchez. 2020. "Summary of Marine and Hydrokinetic (MHK) Composites Testing at Montana State University." Albuquerque, NM: Sandia National Laboratories. SAND2020-9562. https://tethys-engineering.pnnl.gov/sites/default/files/publications/Miller-et-al-2020-MHK-Composites-Testing.pdf.

Murdy, Paul, Jack Dolson, David Miller, Scott Hughes, and Ryan Beach. 2021. "Leveraging the Advantages of Additive Manufacturing to Produce Advanced Hybrid Composite Structures for Marine Energy Systems." *Applied Sciences* 11(3): 1336. https://doi.org/10.3390/app11031336.

Murdy, Paul, and Scott Hughes. 2020. "Investigating Core Gaps and the Development of Subcomponent Validation Methods for Wind Turbine Blades: Preprint." Golden, CO: National Renewable Energy Laboratory. NREL/CP-5000-75249. https://www.nrel.gov/docs/fy20osti/75249.pdf.

Murdy, Paul, Scott Hughes, and David Barnes. 2022. "Characterization and repair of core gap manufacturing defects for wind turbine blades." *Journal of Sandwich Structures & Materials* 24(7): 2083–2100. https://doi.org/10.1177/10996362221122046.

Nunemaker, Jake D., Michael M. Voth, David A. Miller, Daniel D. Samborsky, Paul Murdy, and Douglas S. Cairns. 2018. "Effects of moisture absorption on damage progression and strength of unidirectional and cross-ply fiberglass-epoxy laminates." *Wind Energy Science* 3(1): 427–438. https://doi.org/10.5194/wes-3-427-2018.